# GROWTH AND CHARACTERIZATION OF ZnSnO THIN FILMS ON POLYMERS FOR OLEDs

**A Thesis submitted to**
**The Graduate School of Engineering and Science of**
**İzmir Institute of Technology**
**in Partial Fulfillment of the Requirements for the Degree of**
**MASTER OF SCIENCE**

**in Physics**

**by**
**Merve EKMEKÇİOĞLU**

**June 2019**
**İZMİR**

We approve the thesis of **Merve EKMEKÇİOĞLU**

**Examining Committee Members:**

**Prof. Dr. Gülnur AYGÜN ÖZYÜZER**
Department of Physics, İzmir Institute of Technology

**Assoc. Prof. Dr. Cem ÇELEBİ**
Department of Physics, İzmir Institute of Technology

**Asst. Prof. Dr. Fulya KÖSEOĞLU**
Department of Metallurgical and Materials Engineering
İskenderun Technical University

**28 June 2019**

**Prof. Dr. Gülnur AYGÜN ÖZYÜZER**
Supervisor, Department of Physics
İzmir Institute of Technology

**Prof. Dr. Lütfi ÖZYÜZER**
Head of the Department of Physics

**Prof. Dr. Aysun SOFUOĞLU**
Dean of the Graduate School of
Engineering and Sciences

# ACKNOWLEDGMENTS

First and foremost, I would like to express my sincere gratitude to my supervisor Prof. Dr. Gülnur AYGÜN for the continuous support of research for her encouragement, patience, motivation, enthusiasm, immense knowledge. Her guidance helped me in all time of research and writing of this thesis and so I could not have imagined having a better supervisor and mentor for my master study. Besides my supervisor, I wish to place on records my heartfelt and sincere thanks to Prof. Dr. Lütfi ÖZYÜZER for his contributions of time and ideas to make my work productive and stimulating. His valuable suggestions, comments, and guidance encouraged me to learn more day by day.

I would like to thank the rest members of my thesis defence committee Assoc. Prof. Cem ÇELEBİ and Asst. Prof. Dr. Fulya KÖSEOĞLU for giving suggestions and helpful comments.

I also would like to acknowledge that this project is partially supported by Turkish Aerospace Industries and Teknoma Technological Materials Inc.

Furthermore, I would like to thank Dr. Mehtap ÖZDEMİR for her excellent guidance, continuous support, and understanding throughout my thesis. Her deep insights helped me at various stages of my research.

I am also very thankful to my colleagues from İzmir Institute of Technology and my fellow labmates in OZYUZER Research Group members for the sleepless days we were working together before deadlines, and for all the fun we have had in the last two years.

Last but not least, I would like to thank my family: my parents Nedim and Ayşe for giving birth to me in the first place and supporting me spiritually throughout my life. I want to thank my sister Elvan, my brother Onur and my sister's husband Faruk for supporting every single one of my dreams, no matter how crazy, and for thinking me the world's best physicist. Also, I would like to thank to my dear nephew Efe and niece Elif for bringing endless joy to my life. I am extremely lucky to be blessed with this excellent family.

# ABSTRACT

## GROWTH AND CHARACTERIZATION OF ZnSnO THIN FILMS ON POLYMERS FOR OLEDs

The use of flexible organic light-emitting diodes (OLEDs) in smartphones and televisions with inclined screen shows significant improvements in commercial applications. Recently, flexible OLEDs have been used in lightweight, portable, wearable and even deformable screens, sensors as well as solid-state lighting applications. Under favour of these applications, remarkable developments are observed in the production of flexible electronics. The advantages of OLEDs according to the existing liquid crystal display (LCD) technology are self-emission capability, wide viewing angle, fast response time, simple structure, and low driving voltage. Highly conductive and transparent anodes are required for efficiency and uniform light emission in OLEDs. Indium tin oxide (ITO) which is one of the most promising anodes among transparent conductive oxides (TCO), has superior electrical and optical properties such as ~85% high transmittance at the visible region and ~$10^4$ $\Omega^{-1}$ $cm^{-1}$good conductivity. The reason is due to the bandgap range of about 3.70 eV. Zinc tin oxide (ZnSnO or ZTO) is another TCO commonly used for many applications in the literature. Alternative anodes eliminate the use of ITO due to the absence of indium element so that highly desirable. In this thesis, ZTO is used as anode instead of ITO thin film and the eligibility of ZTO as an anode in OLED production is explored. The advantages of the optimized ZTO thin film according to the ITO are that is abundant on earth, has better performance, has low surface resistance, has less surface roughness, is capable of being produced as an anode in OLEDs. In this thesis to be successful, at the first stage ZTO thin films have grown on soda lime glass by magnetron sputtering, then ZTO and ZTO/Ag/ZTO multilayer thin films respectively have been deposited on flexible Polyethylene terephthalate (PET) and Polyimide (PI) substrates by magnetron sputtering method. In this way, the best coated thin films have been investigated using spectrophotometry, energy-dispersive X-ray spectroscopy (EDS), scanning electron microscopy (SEM), X-ray diffraction (XRD) and Raman spectroscopy.

# ÖZET

## OLED'LER İÇİN POLİMERLER ÜZERİNE ZnSnO İNCE FİLMİNİN BÜYÜTÜLMESİ VE KARAKTERİZASYONU

Eğimli ekranlara sahip akıllı telefonlarda ve televizyonlarda esnek organik ışık yayan diyotlar (OLED'ler) kullanılması, daha çok ticari uygulamalarda önemli gelişmeler göstermektedir. Son zamanlarda, esnek OLED'ler, hafif, taşınabilir, giyilebilir ve hatta deforme edilebilir ekranlarda, sensörlerde ve ayrıca katı hal aydınlatma uygulamalarında kullanılmaktadır. Bunun sonucunda esnek elektronik üretiminde dikkat çekici gelişmeler gözlemlenmiştir. OLED'lerin mevcut sıvı kristal ekran (LCD) teknolojisine gore avantajları, kendi kendine emisyon yetisine sahip olması, geniş görüş açısı olması, hızlı tepki süresi olması, basit yapı ve düşük çalışma voltajıdır. OLED'lerde verim ve homojen ışık emisyonu için, yüksek iletken ve şeffaf anotlar gereklidir. Saydam İletken Oksitler (TCO) ince filmler arasında en umut verici anotlardan olan indiyum kalay oksit (ITO) görünür bölgede ~%85'lik yüksek geçirgenlik ve ~$10^4$ $\Omega^{-1}cm^{-1}$'lik iyi iletkenlik gibi üstün elektriksel ve optiksel özelliklere sahiptir. Bunun nedeni ise yaklaşık 3.70 eV geniş bant aralığından kaynaklanmaktadır. Çinko kalay oksit (ZnSnO veya ZTO) literatürdeki birçok uygulama için yaygın olarak kullanılan bir başka TCO'dur. İndiyumun azlığından dolayı ITO kullanımını ortadan kaldıran alternatif anotlar oldukça arzu edilmektedir. Bu araştırmada ITO ince filmi yerine anot olarak ZTO kullanılmakta ve ZTO'nun OLED üretiminde anot olarak uygunluğu araştırılmaktadır. Optimize edilmiş ZTO ince filmin ITO'ya göre avantajları yeryüzünde bol miktarda bulunması, daha iyi performans göstermesi, düşük yüzey direncine sahip olması, daha az yüzey pürüzlülüğü olması ve OLED'lerde anot olarak üretilebilme kabiliyetine sahip olmasıdır. Bu tezde, amacımıza ulaşmak için ilk olarak ZTO ince filmlerin soda kireç cam üzerine mıknatıssal saçtırma yöntemiyle büyütüldü, sonra sırasıyla ZTO ve ZTO/Ag/ZTO çok katmalı ince filmler esnek polietilen tereftalat (PET) ve Poliimid (PI) alttaşlar üzerine mıknatıssal saçtırma yöntemi ile kaplanmıştır. Böylece, en iyi kaplanan ince filmler, spektrofotometri, enerji dağılımlı X-ışını spektroskopisi (EDS), taramalı elektron mikroskobu (SEM), X-ışını kırınımı (XRD) ve Raman spektroskopisi kullanılarak incelenmiştir.

*To my family…*

# TABLE OF CONTENTS

# LIST OF FIGURES

# LIST OF TABLES

**Table** **Page**

# CHAPTER 1

# INTRODUCTION

## 1.1. Review of Organic Light Emitting Diodes

Attracting interest around the world, research on organic light emitting diodes (OLEDs) have become the most promising displays, lighting and power-saving, it has grown rapidly with the development of amorphous organic semiconductor materials of available today. OLEDs technologies are used for commercial applications to generate digital displays in devices like computer monitors, portable systems and television screens. Also, the commercial applications from the portable systems are contained like smartphones, digital media players, car radios, digital cameras, car lighting, handheld game consoles, and PDAs. The OLED is a light emitting diode (LED) emits light in response to an electric current. The electroluminescence (EL) is the emission of light from materials in an electric field and most of all, it was observed from single crystals of anthracene in 1960 (Helfrich and Schneider 1965). Therefore the EL devices stand for the ultimate generation of light sources, OLEDs was firstly succeeded by Tang in 1986 who used the growth layer of molecular organic material to manufacture green light emission (Tang and VanSlyke 1987). A great invention had consisted when Friend and co-workers reported the first example of an OLED in which the light emitting devices based on the organic macromolecules in 1990 (Burroughes et al. 1990).

Over the last few years, there has been the most important research investment in growth of flexible OLEDs about using in the displays technologies and energy storage devices because their very thin profiles, light and strong display systems, their talent to flexible, twist, fold and roll for ultra-portability, and engineering design afforded by these feature (K. H. Choi et al. 2008). Advanced polymer substrates are necessary for the successful realization of obtaining ultra-performance flexible OLEDs. Therefore, OLEDs are very important to assemble low resistances, immensely flexible and transparent conducting electrodes on the difference polymer substrates (K. H. Choi et al. 2008). Lately, the polymer materials are accepted as the potential candidates as the substrate such as polyethylene naphthalate (PEN), polycarbonates (PC), polyether

sulfone (PES) and polyethylene terephthalate (PET) (Kim et al. 2015). This polymer substrate has great importance potential as an advanced one for flexible OLEDs. Hence, the development of transparent conducting oxide (TCO) films on polymer substrates is violently demanded in flexible OLEDs development and commercialization over the next decade.

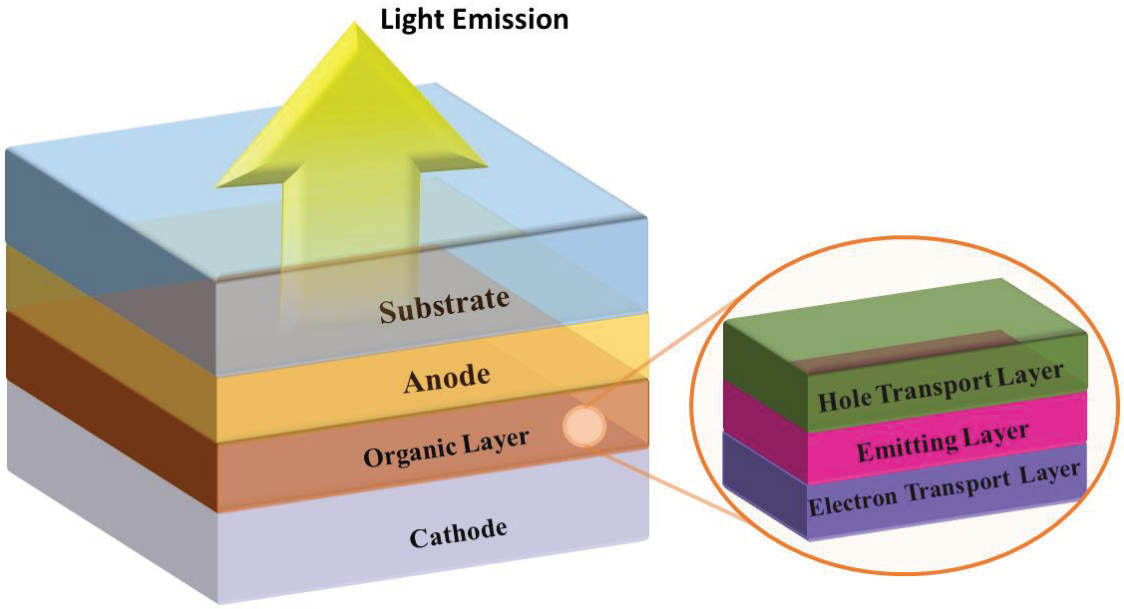


Figure 1.1. The basic structure of OLED.

The basic schematic diagram of a typical OLED is shown in Figure 1.1 (Shirota and Kageyama 2007). The OLED is commonly composed of one or more specialty semiconducting organic thin films that are sandwiched two electrodes, an anode and a cathode organic layer in between of them, all deposited on a substrate, respectively. Thus, these electrodes one of which must be transparent (Hung and Chen 2002).On the other hand, ITO films are the most widely used material as a transparent conducting oxide (TCO). As cathode materials in place of the commonly used low work function metals which is typically aluminium, silver and calcium (Parthasarathy, Liu, and Duggal 2003). Depending on their applications, OLEDs structures usually can differ from one to another. For example, in order to increase efficiency, the conductive properties and the operational stability, the advanced layer structures like three-layer organic electroluminescent structure shown in Figure 1.1 have been uncovered. It contains an organic emission layer sandwiched between the hole transport layer and the electron transport layer ETL, designated HTL/EML/ETL. The thickness of the organic layer in

each case is very thin, between 100 nm and 200 nm because of the low carrier mobility (Thejo Kalyani and Dhoble 2015).

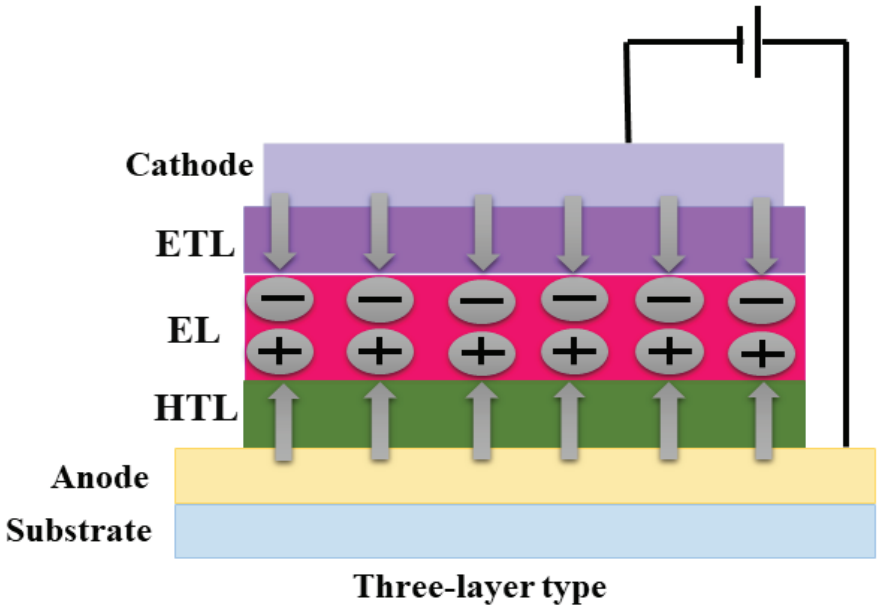


Figure 1.2. The basic configuration of OLED.

OLEDs run on the principle of electroluminescence. For the basic configuration of OLED, by applying a voltage (typically < 10 V) to such an OLED electrical current flows between the electrodes, electrons will move from cathode to anode through organic layers, which is depicted as Figure 1.2. Electrons are transported through the lowest unoccupied molecular orbital (LUMO), while holes are transported through the highest occupied molecular orbital (HOMO). Thus, as the anode is to a large extent positive electrical potential from the cathode, injection of holes come about the anode into the HOMO of HTL to the contrary the electrons are injected from the cathode into the LUMO of ETL. Photons produced from the organic layers radiate through the glass substrate and spread out to the air for light emission. So, the working principle of an OLED is also described (Shirota and Kageyama 2007).

## 1.2. The Purpose of This Thesis

The aim of the work described in this thesis was to growth and characterization of ZnSnO (ZTO) thin films on polymers for OLEDs. Highly conductive and transparent anodes are necessary for efficiency and uniform light emission in OLEDs. In this study, ZTO is used as anode instead of ITO thin film and the eligibility of ZTO as an anode in

OLEDs production is explored. The advantages of the optimized ZTO thin film according to tin-doped indium oxide (ITO) are that is abundant on earth, has better performance, has low surface resistance, has less surface roughness, is capable of being produced as an anode in OLEDs. To achieve sheet resistance and high transmittance for our ZTO thin films, various characterization techniques should be used in my thesis. In my thesis, we suggested for the sheet resistance and optical transmission ZTO/Ag/ZTO multilayer electrodes in addition to growing ZnSnO in the cost-efficient transparent conductive oxides for OLEDs. The control of the thickness and morphology of the Ag layer is critical to enhancing the transmission and the sheet resistance of the ZTO/Ag/ZTO multilayer thin film electrodes. Spectrophotometry, scanning electron microscopy (SEM), energy dispersive X-ray spectroscopy (EDX or EDS), X-ray diffraction (XRD) and Raman spectroscopy are characterization techniques to define as-growth ZTO thin films on polymers for OLEDs. The aims of this thesis are to:

- ✓ Deposition accomplished by two different targets: one of them is $Zn_2Sn$ (ZT) and the other one is ZnSnO (ZTO) to investigate the lowest sheet resistance *($R_{sh}$)* and the highest optical transmittance.
- ✓ Researching the structural, electrical and optical properties of ZnSnO and ZTO/Ag/ZTO thin films.
- ✓ The optimization of ZTO/Ag/ZTO multilayer thin film is made for improvement of OLEDs.

# CHAPTER 2

# LITERATURE REVIEW

## 2.1. Transparent Conducting Oxides

The transparent conducting oxides (TCOs) was reported by Badeker when he first achieved the conducting property of CdO thin films prepared by sputtering cadmium in 1905 (Bädeker 1907). The unique properties such as the good electric conductivity and high optical transparent depend on the thin films of TCOs have the most common applications that continue to develop day by day. Generally, tin-doped indium oxide (ITO), fluorine-doped $SnO_2$ (FTO), aluminum-doped ZnO (AZO), and cadmium stannate ($Cd_2SnO_4$), are very often used TCO materials for various applications (Zeng et al. 2003). The world is one of the fastest growing electronics markets. Therefore, TCOs have turned into necessary components in a multitude of modern devices with the inclusion of solar cells, portable electronics, transparent heaters, touch screens, optics, sensors, multi-functional windows, flexible electronics and flat-panel displays. Most of these applications could be developed transparent conducting oxide of more activities (Ginley 2011).

### 2.1.1. General Properties of TCO

Majority of the beneficial oxide-based materials are n-type conductors that have a wide-bandgap oxide semiconductors bandgap of >3 eV and transparent conducting oxides have high optical transmittance at certain 400-700 nm and high electrical conductivity because it is frequently induced by doping another element. Thus, TCO materials are that the optical transmittance of around 80% in the visible region as well as a low electrical resistivity of around $10^{-3}$-$10^{-4}$ Ω cm (Lewis and Paine 2000). Therefore, the most commonly used TCO thin films for optoelectronic device applications has been indium tin oxide, $In_2O_3$:Sn[1] typically called tin-doped indium oxide or ITO, since the 1960s. ITO has largely used due to its inapproachable electrical conductivity and optical properties like the best conductivity ($10^4$ $\Omega^{-1}$ $cm^{-1}$) and high

transmittance (~85%) at 400-700 nm in so far as its large bandgap of about 3.70 eV (Tuna et al. 2010).

Table 2.1. History of processes and for references making TCOs (Source: Ginley 2011).

| Material | Year | Process | Reference |
|---|---|---|---|
| *Cd-O* | | | |
| CdO | 1907 | Thermally Oxidation | K. Badeker, Ann. Phys. (Leipzig) 22, 749 (1907) |
| Cd-O | 1952 | Sputtering | G. Helwig, Z. Physik, 132, 621 (1952) |
| *Sn-O* | | | |
| $SnO_2$:Cl | 1947 | Spray pyrolysis | H.A. McMaster, U.S. Patent 2,429,420 |
| $SnO_2$:Sb | 1947 | Spray pyrolysis | J.M. Mochel, U.S. Patent 2,564,706 |
| $SnO_2$:F | 1951 | Spray pyrolysis | W.O. Lytle and A.E. Junge |
| $SnO_2$:Sb | 1967 | CVD | H.F. Dates and J.K. Davis, USP 3,331,702 |
| *Zn-O* | | | |
| ZnO:Al | 1971 | | T. Hada, Thin Solid Films 7, 135 (1971) |
| *In-O* | | | |
| $In_2O_3$:Sn | 1947 | | M.J. Zunick, U.S. Patent 2,516,663 |
| $In_2O_3$:Sn | 1951 | Spray pyrolysis | J.M. Mochel, U.S. Patent 2,564,707 (1951) |
| $In_2O_3$:Sn | 1955 | Sputtering | L. Holland and G. Siddall, Vacuum III |
| $In_2O_3$:Sn | 1966 | Spray | R. Groth, Phys. Stat. Sol. 14, 69 (1969) |
| *Ti-O* | | | |
| $TiO_2$:Nb | 2005 | PLD | Furubayashi et al., Appl. Phys. Lett. 86, 252101 (2005) |
| *Zn-Sn-O* | | | |
| $Zn_2SnO_4$ | 1992 | Sputtering | Enoki et al., Phys. Stat. Solid A 129, 181 (1992) |
| $ZnSnO_3$ | 1994 | Sputtering | Minami et al., Jap. J. Appl. Phys. 2, 33, L1693 (1994) |
| a-ZnSnO | 2004 | Sputtering | Moriga et al., J. Vac. Sci. & Tech. A 22, 1705 (2004) |
| *Cd-Sn-O* | | | |
| $Cd_2SnO_4$ | 1974 | Sputtering | A.J. Nozik, Phys. Rev. B, 6, 453 (1972) |
| a-CdSnO | 1981 | Sputtering | F.T.J. Smith and S.L. Lyu, J. Electrochem. Soc. 128, 1083 (1981) |
| *In-Zn-O* | | | |
| $Zn_2In_2O_5$ | 1995 | Sputtering | Minami et al., Jap. J. Appl. Phys. P2 34, L971 (1995) |
| a-InZnO | | | |
| *In-Ga-Zn-O* | | | |
| $InGaZnO_4$ | 1995 | Sintering | Orita et al., Jap. J. Appl. Phys. P2. 34, 1550 (1995) |
| a-InGaZnO | 2001 | PLD | Orita et al., Phil. Mag. B 81, 501 (2001) |

Among the various TCO materials have accepted substantial attention include tin oxide ($SnO_2$) commonly doped with fluorine, and cadmium stannate ($Cd_2SnO_4$), which is inherently doped. Table 2.1 clearly shows that is the wide diversity of a list of current historically significant innovations in the TCO materials with references compiled (Ginley 2011). In additionally, the majority carrier is electrons or holes and the conductors are classified in n-type or p-type. The literature review shows that TCOs have developed to contain the individual oxides of In, Cd, Sn, Ga, and Zn, even their

alloy mixtures and compounds (Pasquarelli, Ginley, and O'Hayre 2011). Figure 2.1 is shown in the TCOs composition space. Also, the lines are amongst two oxides at edges (binary systems), the areas are between three oxides at faces (ternary systems) and individual oxides are located at the corners (Pasquarelli, Ginley, and O'Hayre 2011). Appreciable values of electrical conductivity had been examined in many single, binary, ternary and quaternary metal oxide systems since the discovery. From the practical standpoint, it is desirable to develop TCO materials that are amorphous because uniform films over large areas are desirable and amorphous layers are better suited to accommodate strain which is the necessary condition for enabling flexible electronics applications (Exarhos and Zhou 2007).

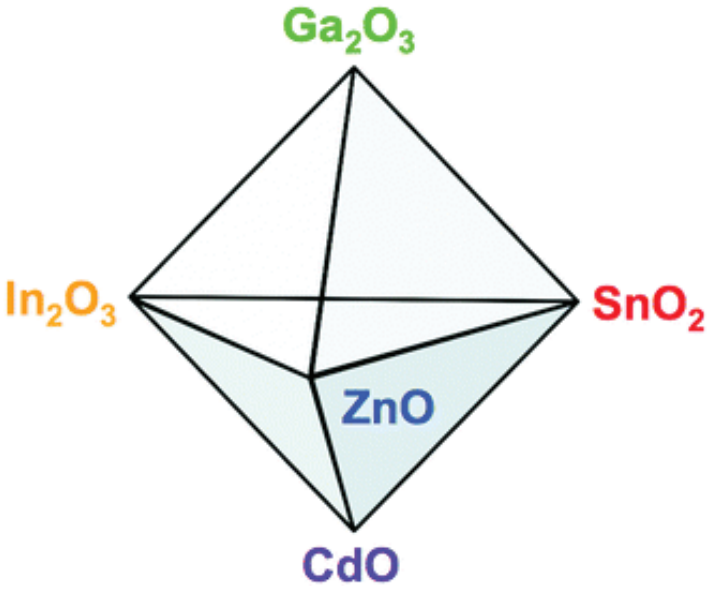


Figure 2.1. Composition space for conventional TCO materials
(Source: Pasquarelli, Ginley, and O'Hayre 2011).

Figure 2.2 clearly shows the comparison of the abundance for the dopants and TCO cations. The common TCO cations are highlighted by coloured circles with additional possible dopants shown with squares. Currently, because of indium's rarity and thus high price, there is great interest in non-indium based TCOs. Furthermore, ITO films and other thin films the standard is detected by various factors like the thickness surface morphology, the optically transparent, uniformity and electrical conductivity. Moreover, the deposition technologies, operation conditions and post-deposition thermal treatments influence the entire optical and electrical properties of ITO films. Hence, alternative anodes that eliminate its use are highly desired owing to the scarcity

of indium. In this research ZTO has been used as a replacement of ITO and its appropriate candidacy as an anode in OLED production has been explored.

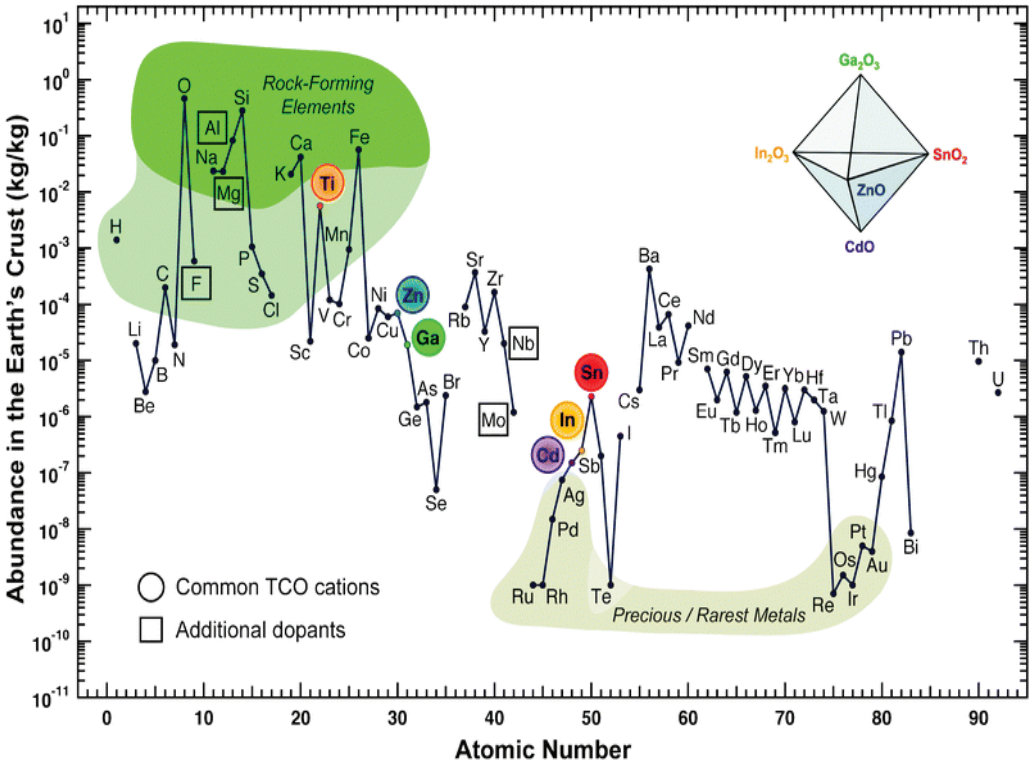


Figure 2.2. Comparison of the abundance for different TCO materials (Source: Pasquarelli, Ginley, and O'Hayre 2011).

## 2.1.2. Electrical Conductivity and Resistivity of TCO

In general, the electronic properties of materials are necessitated to understand that the electrical conductivity is a very property of TCOs. The most substantial electrical feature of solid materials their resistance to flow of electrical current. Many published literature discusses the electrical properties of TCOs in terms of resistivity *(ρ)*, which is the reciprocal of conductivity *(σ)* and has units of Ω cm. The materials have low resistivity provided that the electrons flow with ease through these materials. Electricity has large hardship flowing through a material, so material has high resistivity. Conductivity is the opposing of resistivity which is the inverse of electrical conductivity to describe. So, the high electrical resistivity is identical with low electrical conductivity (Ghorbani and Taherian 2019):

$$\sigma = \frac{1}{\rho} \tag{2.1}$$

The substrate temperature and the applied magnetic field of materials depend on the electrical resistivity of the materials. In Figure 2.3, the material features are isotropic in directions and homogeneous in regions. Electrical resistivity *(ρ)* can describe as follows:

$$E = \rho J \tag{2.2}$$

where the electric field is shown $E$, the current density is shown $J$ and the resistivity is shown $\rho$. The electric field $E$ is offsetting by the voltage of $V$ divided by the distance of $d$ over the voltage is adopted. Equation *(2.3)* is shown another form of Ohm's law equation.

$$E = \frac{V}{d} \tag{2.3}$$

In the sample supposed that materials are homogeneous, therefore the electrical resistivity of $\rho$ is a scalar magnitude. As shown in Figure 2.3, is taking into account the sample in consequence of the current density of $J$ is described by:

$$J = \frac{I}{A} \tag{2.4}$$

To analyse material is bounded by two electrodes with the area of $A$, in order to place apart from another material with the distance of $d$, as shown in Figure 2.3. Combining the equations *(2.1)*, *(2.2)*, and *(2.3)* and rearranging gives:

$$V = I\frac{\rho d}{A} \tag{2.5}$$

From Ohm's law, $R$ is even to the voltage across the material divided by the current. The resistance between the two ends is given by:

$$R = \rho\frac{d}{A} = \rho\frac{d}{tw} = \frac{\rho}{t}\frac{d}{w} \tag{2.6}$$

$\frac{\rho}{t}$ should have units *(ohms)* since $\frac{d}{w}$ has no units. However, $\frac{\rho}{t}$ is not the resistance of sample. To distinguish between $R$ and $\frac{\rho}{t}$, the ratio $\frac{\rho}{t}$ is given the units *(ohms/square)* and is named sheet resistance, $R_{sh}$. Hence the resistance of sample can be written as:

$$R = R_{sh}\frac{d}{w}\ ohms \tag{2.7}$$

$$R_{sh} = \frac{\pi}{(In2)}\frac{V}{I} = 4.53\frac{V}{I} \tag{2.8}$$

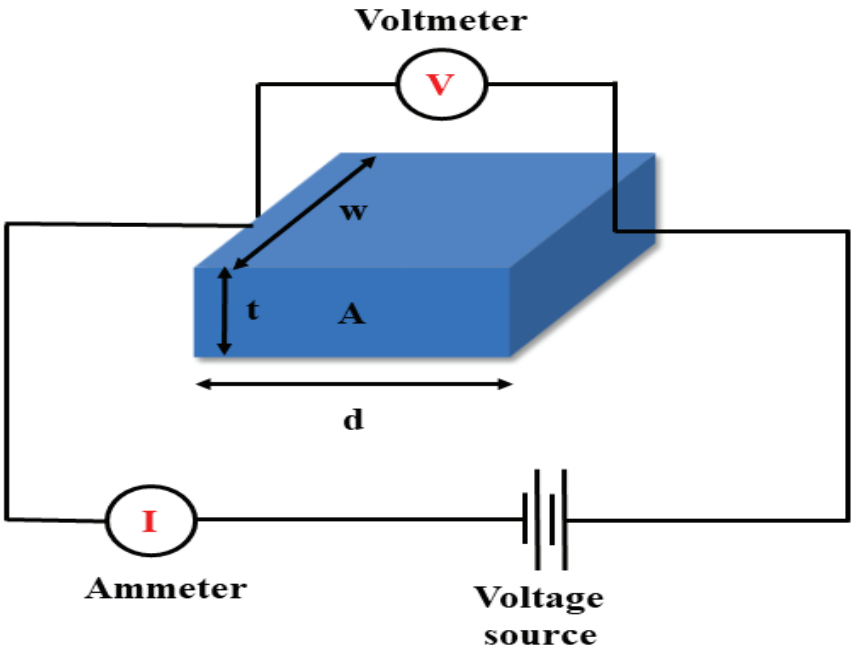


Figure 2.3. Simple technique for measuring the resistivity.

There are several correction factors such as geometry should be inputted to get a much accurate and precise value of the sheet resistance ($R_{sh}$). The electrical resistance of sample relies on the geometry of the sample. In this way, the electrical resistance $\rho$ is independent of the sample size or the sample shape. The electrical conductivity is easily related to the free electron density by:

$$\sigma = \frac{ne^2\mu}{m^*} \tag{2.9}$$

where the mass electron is $m^*$, the number of electrons is $n$ per unit volume carrying current in the sample, the electrons charge is $e$, and the average interval between clashes for a single electron is $\mu$. If the mass of the electron is increased, their movement will be decreased and taken extended to get through samples (Ghorbani and Taherian 2019).

### 2.1.3. Optical Properties of TCO

In the n-type TCOs, the optical properties are determined not only by the optical transitions between the valence bands and conduction bands but also between the occupied conduction states and the other conduction band states. The important optical characteristic of TCOs transmission *(T)*, absorption *(A)* and reflection *(R)* could be detected via its geometry consists of, refraction index $n$, band gap $E_g$ and extinction coefficient $k$. So, geometry in measuring film surface roughness, film thickness and thickness uniformity. While the geometry of thin film is extrinsic, which relying on the chemical composition and material is that the intrinsic are $T$, $A$, and $R$ (Wei and Segev 2005).The semiconductor band theory can be established the induction of electrical properties of TCOs. The electrical conduction becomes inside the semiconductor material, so the absorbed Photon energy must be induced the valence band maximum $(VB_{max})$, the conduction band minimum $(CB_{min})$, respectively. The electron is induced into conduction in order to require the higher energy photon for a wider band gap. For this reason, in order to decrease the odds of stimulant the electron into the conduction, in a material expands at the band gap $E_g > 3.0$ eV while establishing a large separation from $VB_{max}$ to $CB_{min}$ of the material, then permitting transparency at the visible portion. Furthermore, Transparent conducting oxides have been advanced by doping materials so as to make easy the charge carrier generation within the structure. In the description of the band, the model has a prominent difference from the basic band gap (the low energy shift effect on the bulk HOMO) to the optical band gap (an extrinsic property) which corresponded to allow the minimum energy for an optical transition (Dsy and Peiris 2018). The optical band gap detects the transparency of a material which is important in TCO applications. In order to achieve n-type conducting properties, electrons are injected from the ionized donors straight in the valence band. Figure 2.4 shows that there is orbital overlap, it would permit delocalization of electrons from the defect sites such that $CB_{min}$ filled up electronic states, in other words, the $CB_{min}$ down

below Fermi level shifts. It is known as an effect that the Moss–Burstein shift is efficaciously enlarged the optical bandgap.

$$E_g = E_{CB_{min}} - E_{VB_{max}} \tag{2.9}$$

to

$$E_g^{opt} = E_g^{MB} + E_g = E_F - E_{VB_{max}} \tag{2.10}$$

Moss–Burstein shift:

$$E_g^{MB} = E_F - E_{CB_{min}} \tag{2.11}$$

where the optical band gap of $E_g^{opt}$ is permitted the optical transition between the VB and the CB, the fundamental energy gap of $E_g$ is separated from $VB_{max}$ and $CB_{min}$ , the Moss-Burstein shift is $E_g^{MB}$ and The Fermi energy level is $E_F$. Thus, TCOs of the lattice defects will be increased both optical transparency and electrical conductivity.

The optical band gap is a very considerable direction in designing TCO. The next electronic energy level $(CB_{min+1})$ and the conduction band level is different which a broad interval is 3.0 eV. So, undesirable optical absorption prevents excited electron (Dixon et al. 2016). Range of visible transmission window of the TCO films growth on substrate is affected via the optical parameters and properties. On the other hand, the refractive index $n_{sub}$ of the most widespread substrates is a refractive index approximately ~1.45 for fused silica has a refractive index approximately ~1.6 for various glasses. Various interference bands were formed in order to manufacture minimal and maximal values is $T$ which the wavelength and thickness have differed 100 nm thicker (Major and Chopra 1988). Furthermore, the maximum transmission is in air, $T_{max}$=90% and 93% for the coated films on glass and fused silica, respectively. The minimum transmission $(T_{min})$ in air is cleared by (Castañeda 2011):

$$T_{min} = \frac{4n^2 n_{sub}}{(1+n^2)(n^2+n_{sub}^2)} \tag{2.12}$$

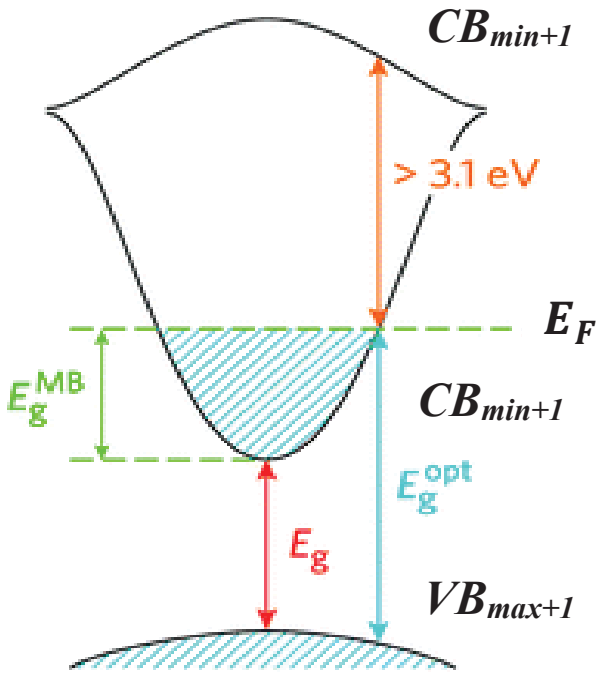


Figure 2.4. Graph of the Moss–Burstein shift
(Source: Dixon et al. 2016).

The refractive index for most TCOs resides in the visible range of *n=1.8-2.8* and gives at least transmission within the range of $T_{min}$*=0.5–0.8*. Minimum transmission may be approximated from equation.

$$T_{min} = 0.051n^2 - 0.545n + 1.654 \quad (2.13)$$

In the visible spectrum as refractive index decreases or increasing wavelength affects optical transmission minimum increases. Although the extinction coefficient has a significant effect on the transmission $T_{maximum} < T_{substrate}$, the optical transmission minimum of decrease. In this way, TCO the film will decrease depending on thickness, the optical transmission will increase. For this reason, the sheet resistance will show an increase.

## 2.2. What is Zinc Tin Oxide (ZTO)?

Non-centrosymmetric ternary oxides display unique symmetry-dependent and spontaneous polarization properties, which are technologically important for applications in ferroelectricity, piezoelectricity, and nonlinear optics. Zinc stannate is a

ternary oxide of zinc (Zn) and tin (Sn) and thus also known as zinc tin oxide (ZnSnO or ZTO). Moreover, zinc stannate or metastannate ($ZnSnO_3$) and zinc orthostannate ($Zn_2SnO_4$) are the two compound forms that exist in the ZTO system. So, metastannate is face centered perovskite, while orthostannate forms an inverse spinel structure ($AB_2O_4$ type), as shown in Figure 2.5. (Bora et al. 2015). Zinc tin oxide has a high optical band gap of >3 eV which provides the material highly transparent to visible light.

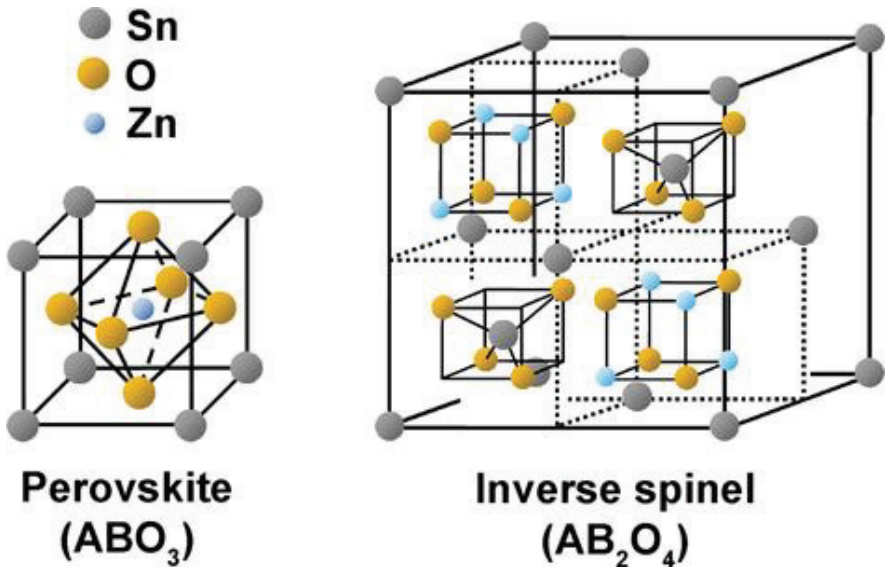


Figure 2.5. Crystal structures of face centered perovskite and inverse spinel (Source: Bora et al. 2015).

Zinc tin oxide is an n-type semiconductor, therefore, its stoichiometry is the most generally defined like $(ZnO)_x(SnO_2)_{1-x}$ (0<x<1). Trigonal ilmenite $ZnSnO_3$ and cubic spinel $Zn_2SnO_4$, two crystalline forms have been noticed. Using ZTO as an environmentally friendly replacement for the industry standard materials in these applications (ITO, CdS) can reduce the production costs and potentially improve device performance (H. Q. Chiang et al. 2005). Transparent conductive oxides are an essential component in many products such as flat panel displays, photovoltaic devices and organic light emitting diodes. Although the binary oxides such as ZnO, $SnO_2$ and $In_2O_3$ find numerous applications, recently, spinel type cadmium stannate ($Cd_2SnO_4$) has been identified as one of the best candidates for TCO applications due its promising electrical and optical properties. Other materials, the oxides of indium, tin and zinc are currently the most commercially important TCOs. In spite of their large band gap, which makes them transparent under normal conditions; they can sustain a high concentration of

carrier electrons with a high mobility (Stambolova et al. 1997). Development of these and other TCO semiconductors is important because the expanding need for transparent electrodes for optoelectronic device applications is jeopardizing the availability of indium-tin-oxide (ITO), whose main constituent, indium, is a very expensive and scarce material. ZTO semiconductors are promising as alternatives to ITO for thin-film transparent electrode applications (Minami 2005). There are many conductivity and mobility values for transparent conductive oxides in the literature, improving on the film composition and growth technique.

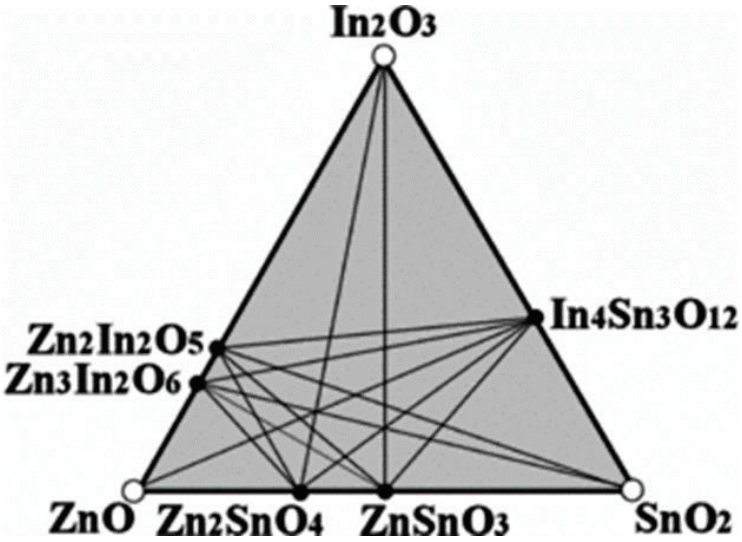


Figure 2.6. TCO semiconductors for thin film transparent electrodes (Source: Minami 2005).

With the purpose of obtaining highly transparent and conductive ZnO films, it has been reported that tin doping ZnO films prepared by rf magnetron sputtering was not effective (Minami 2005). In addition to that research into ZTO and other multi metal oxide thin films have drawn increased attention in the past decade. Moreover, TCO semiconductors like impurity-doped ZnO, $In_2O_3$ and $SnO_2$ and multi-component oxides composed of combinations of these binary compounds are the best candidates for practical use, as shown in Figure 2.6 (Minami 2005). In respect of a promising alternative to ITO films from researches, oxide/metal/oxide the multilayer thin films have been proposed to obtain lower resistivity than $10^{-4}\Omega$ cm of ITO thin films (Welzel and Ellmer 2012). In a recent study, Koseoglu et al. observed that the effect of electro-annealing in air and vacuum on the optical and electrical properties of ITO thin films grown by large area DC magnetron sputtering at 250 $^{o}$C substrate temperature (Koseoglu

et al. 2015). In particular, ZTO thin films, with low resistivity and source materials that are inexpensive and non-toxic, are the best candidates. Besides, further development of the deposition techniques, such as magnetron sputtering as well as of the targets is required to enable the preparation of ZTO thin films on polymer substrates with less surface roughness. In the study of Demirhan et al. that in order to coat of ITO thin films on PET substrate without heating were made, using a roll to roll large area DC magnetron sputtering system. As a result of depending on the oxygen gas flow rate, the effect of growth conditions has been investigated in the thin film properties which is specifically resistivity and transparency (Demirhan et al. 2020). Schmidt et al. observed that oxide/metal/oxide multilayer electrodes have been explored as transparent conducting electrode, which has deposited at room temperature. ZTO/Ag/ZTO (ZAZ) multilayer thin film electrodes found sheet resistance of 6 Ω/□ and optical transmittance 82% at 550 nm in this way, this research was first submitted for applications to conductive electrodes (Schmidt et al. 2011).

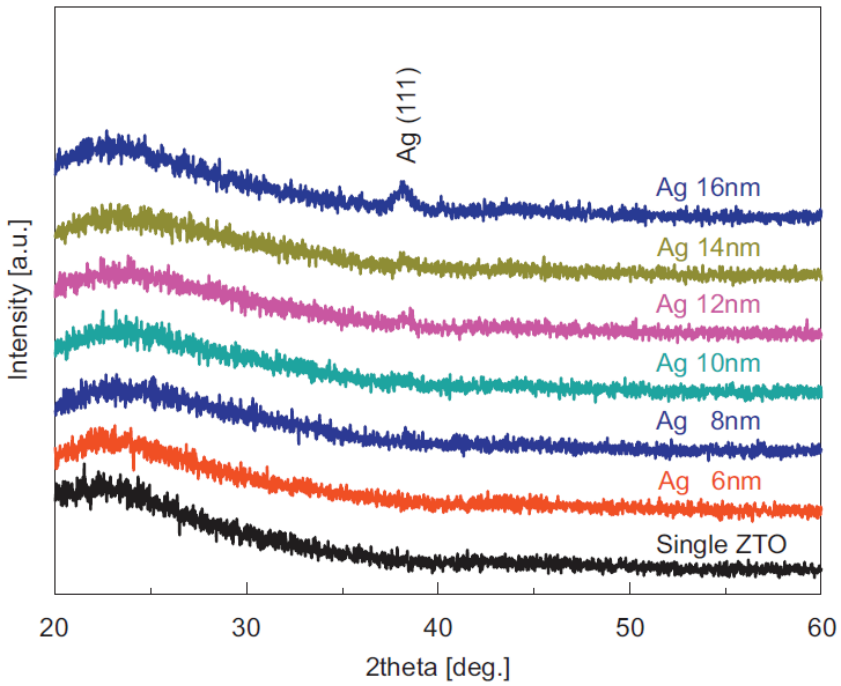


Figure 2.7. XRD plots of the ZAZ/SLG multilayer as a function of Ag thickness (Source: Y. Y. Choi et al. 2011).

In the study of Choi et al. flexible dielectric/metal/dielectric (DMD) multilayers like roll to roll grown flexible $ZnSnO_3$/Ag/$ZnSnO_3$ have been reported as candidates for flexible ZTO electrodes owing to their low cost, low sheet resistance, high optical transmittance, and good flexibility. Also, due to the high cost of indium element, zinc

tin oxide is preferred (Y. Y. Choi et al. 2011). Moreover, XRD plots of the ZTO/Ag/ZTO multilayers with increasing Ag thickness, to investigate the microstructural properties of ZTO/Ag/ZTO multilayer thin film electrodes, as shown in Figure 2.7. Up to a thickness of 8 nm, there was no peak related to crystalline Ag or ZTO. A crystalline Ag (111) peak started to appear at an Ag metal layer thickness of 10 nm. Recently, in the study of Seok et al. ZnSnO/AgPdCu/ZnSnO (ZTO/APC/ZTO) multilayer thin film electrode that have grown on 1500 mm PET using mass-production-scale roll-to-roll (RTR) sputtering at room temperature without breaking vacuum as shown in Figure 2.8.

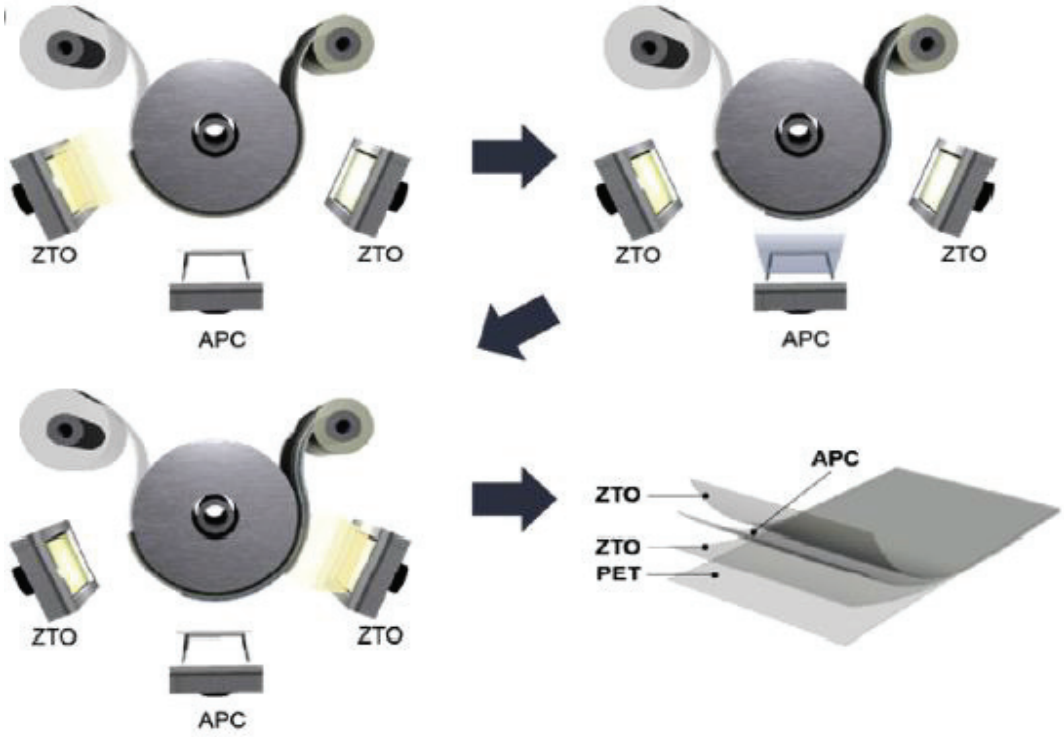


Figure 2.8. Schematic of the continuous RTR sputtering process
(Source: Seok et al. 2019).

In addition to this ZTO/APC/ZTO multilayer on PET substrate is found the sheet resistance of 3.43 Ω/□ and the optical transmittance of 80.99% (Table 2.2). In comparison, the optical transmission results of the optimal thickness values ZTO (20 nm)/APC (14 nm)/ZTO (15 nm) multilayer and 125-nm-thick reference ITO thin films sputtered on PET substrates at room temperature. Here, ITO thin film has shown sheet resistance of 40.25 Ω/□ and resistivity of $5.03 \times 10^{-4}$ Ω cm. Compared to the reference ITO thin film, the ZTO/APC/ZTO multilayer reduced sheet resistance of 3.43 Ω/□ and resistivity $1.68 \times 10^{-5}$ Ω cm. Besides, the use of an Ag-Pd-Cu alloy interlayer has the

identical metallic conduction such as Ag and improves durability against heat and humidity because the Cu and Pd alloy elements reduce the surface diffusion of Ag atoms.

Table 2.2. Electrical and optical properties of the optimized ZTO/APC/ZTO multilayer thin film electrode, and reference ITO (Source: Seok et al. 2019).

| | ITO | ZTO/APC/ZTO |
|---|---|---|
| **Sheet Resistance (Ω/□)** | **40.25** | **3.43** |
| **Resistivity (ohm cm)** | $5.03 \times 10^{-4}$ | $1.68 \times 10^{-5}$ |
| **Mobility ($cm^2/V\ s$)** | 25.18 | 4.15 |
| **Concentration ($cm^{-3}$)** | $4.93 \times 10^{20}$ | $8.99 \times 10^{22}$ |
| **Transmittance at 550 nm (%)** | 84.07 | 80.99 |

ZTO/APC/ ZTO multilayer thin film electrodes, the highly conductive APC interlayer causes low resistivity, and DMD structure can prevent reflections from the APC layer to produce the high optical transmittance. In addition, the low IR transmittance and high reflection of the APC metal layer have been caused effective heat shielding by the ZTO/APC/ZTO multilayer thin film electrode. Based on bending, twisting, rolling, and folding tests, they have been confirmed the outstanding mechanical flexibility of the ZTO/APC/ZTO electrodes (Seok et al. 2019).

# CHAPTER 3

# EXPERIMENTAL DETAILS

Experimental details can be divided into two parts. The first part consists of thin film growth including the experimental details such as substrate preparation, deposition method of thin films. Moreover, the focus of this part, ZTO thin films were deposited on soda-lime glass (SLG), polyethylene terephthalate (PET) and Polyimide (PI) substrates by DC magnetron sputtering system using $Zn_2Sn$ (ZT) target and ZnSnO (ZTO) target. In the second part, the analysis and characterization techniques of those properties have been explored the physics of the film mechanisms like Profilometry, four-point probe, spectrophotometry, scanning electron microscopy (SEM), X-ray diffraction (XRD), Raman spectroscopy. For this reason, in the steps of growth and characterization of ZTO thin films on Polymers for OLED, it will be optimized to coat ZTO thin film appropriate parameters such as pressure, target-substrate distance, deposition time, etc. As a result, the annealing temperatures and the deposition parameters will determine in order to obtain in the lowest sheet resistance and the highest optical transmission.

## 3.1. Growth of ZnSnO Thin Films

In my thesis, the growth of ZnSnO thin films can be divided into four parts. Firstly, polymer substrates are very important to clean for using ZTO as an anode in OLED production so substrates preparation is to be expounded. Other parts, many experimental details have been tried to optimize the sputtering conditions and the different substrate temperature or room temperature parameters to get ZTO thin films with desired properties using $Zn_2Sn$ (ZT) target and ZnSnO (ZTO) target. Despite the differences in the various parameters, device structures of the many transparent conductive oxides are shown similar and the schematic cross-section of thin films structure is shown in Figure 3.1. (a). Primarily, After the thin films are deposited on ZTO/SLG samples using $Zn_2Sn$ target, which is the lowest sheet resistance but at the same time high transmittance at 550 nm, they become ready for the characterization

techniques. After the thin films are deposited on ZTO/SLG samples, which is the lowest sheet resistance but at the same time high transmittance at 550 nm, they become ready for the characterization techniques. Aim of using soda-lime glasses substrates is to create homogeneous films by optimizing thin film. As shown in Figure 3.1. (b), ZTO/Ag/ZTO (ZAZ) multilayer thin film electrodes growth have been presented in a number of different parameters for low sheet resistance and high optical transmittance. Actually, the top side of the films is covered with Silver as interlayer by magnetron sputtering technique to form multilayers for the lowest sheet resistance measurements. In the next chapter, the optimization parameters will be given for the growth of ZTO thin films and ZTO/Ag/ZTO electrodes as transparent conductive oxides used to appropriate candidacy as an anode in OLED production.

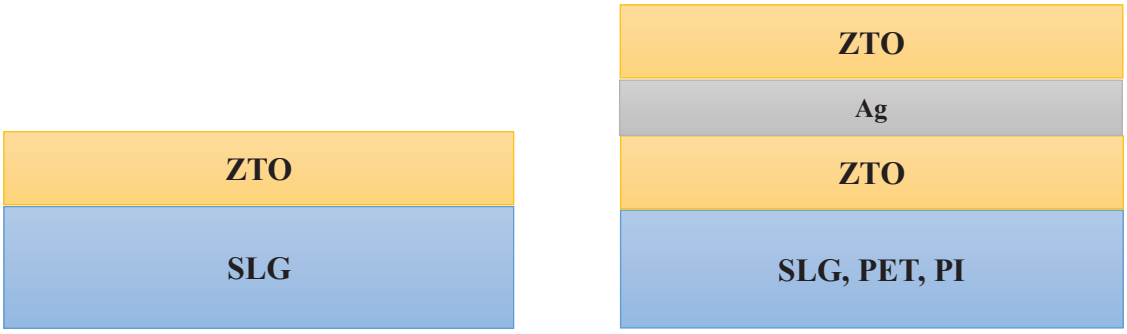


Figure 3.1. (a) Device Structure of ZnSnO thin films using $Zn_2Sn$ target (b) ZAZ multilayer thin film electrodes using ZnSnO target.

### 3.1.1. Substrate Preparation

In this work, the reason for the usage of SLG substrate as-growth of ZTO thin films was that it must be resistant to substrate temperature to apply the substrate heating process. SLGs were respectively cleaned in an ultrasonic bath in acetone, alcohol and de-ionized water for 10 minutes in each, after that as the cleaning of the substrate was accomplished by oxygen plasma etching on account of 10 min to eliminate organic residual. As a result of polymer substrates are very important to assemble the eligibility of ZTO as an anode in OLED production is obtained the reasonable usage of polymer (PI, PET) substrates which have been cleaned with steps except for acetone.

### 3.1.2. Deposition Method of ZnSnO Thin Films

Deposition methods as growth thin films are listed such as chemical vapour deposition (CVD), physical vapour deposition (PVD), thermal evaporation, reactive thermal evaporation, sol-gel process, spray pyrolysis, radio frequency (RF) magnetron sputtering and direct current (DC) magnetron sputtering. Among these methods, DC magnetron sputtering method is the most preferred technique because of having a high accumulative speed and also to get high-quality thin films (Granqvist and Hultåker 2002). In the DC magnetron sputtering, target material particles linear motion of electrons is perpendicular to both electrical and magnetic field to accelerate ambient ionized Argon atoms. In this way, ion concentration on target can be increased. The incident ion undergoes atomic and electronic interactions thus within transition of particles from target (cathode) material to substrate (anode) a thin layer is formed (Ellmer and Mientus 2008). Thin film growth is possible with this method. Figure 3.2 (a) illustrates the picture of DC magnetron sputtering system. Glow discharge which we call plasma can be seen in Figure 3.2 (b), the substrate holder on top of plasma can be placed. The DC magnetron sputtering system used in this thesis was used to sputter ZnSnO thin films in order to be a popular method for coating high-quality thin films.

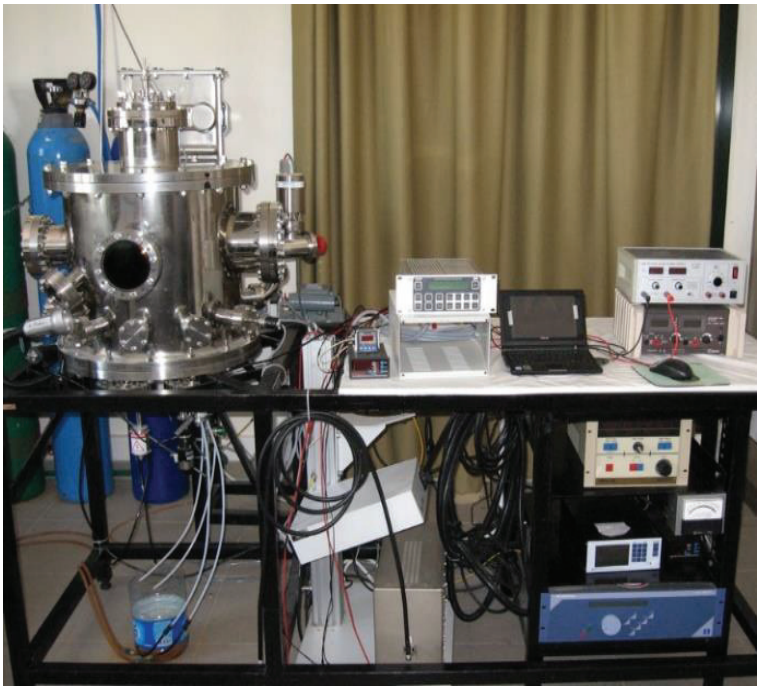

(a)

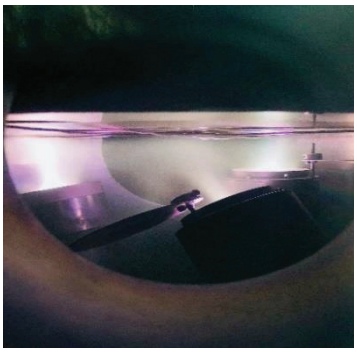

(b)

Figure 3.2. (a) The picture of DC magnetron sputtering system (b) purple colours of plasma, during deposition process.

The sputtering system equipped with a turbo molecular pump and a rough pump had a two-stage pumping system. That's why, the evacuation system to below $2.0x10^{-6}$ Torr, we pumped the rough pump (RP) and then backing the turbo molecular pump (TMP). Also, the target-substrate distance was 7 cm. In additionally, heat-treatment was achieved with top ampoule heating. Then, during the deposition of ZTO thin films, the substrate temperature was checked by a thermocouple. To evaluate base pressure of the system, a cold cathode gauge is used. The content of sputtering gases introduced was controlled by a separate mass flow control (MFC) by which channel 1 controlled the amount of Argon (Ar), channel 2 controlled the amount of oxygen ($O_2$). The MFCs are available to measure gas flow rates from about 0.1 sccm (Standard Cubic Centimeters per Minute). During deposition, baratron is used to measure pressure of vacuum chamber. The sample holder was rotated in order to obtain better surface homogeneous of the coated layer, during the deposition of ZTO films.

### 3.1.3. Heat Treatment of ZnSnO Thin Films

Heat treatments can be controlled the properties of the thin films by the heat treatment steps. For example, heating of a material over a long time span that enables strains and cracks to be removed or at least can provide stress relaxation inside the material. In additional is briefly that used to define all of the controlled heating and cooling operations performed on a material in the thin film for the purpose of altering its microstructure and properties. The focus of this discussion also allows atoms to diffuse inside the structure and rearrange itself to form the crystalline structure by annealing. Figure 3.3 clearly shows that schematic representation of tube furnace.

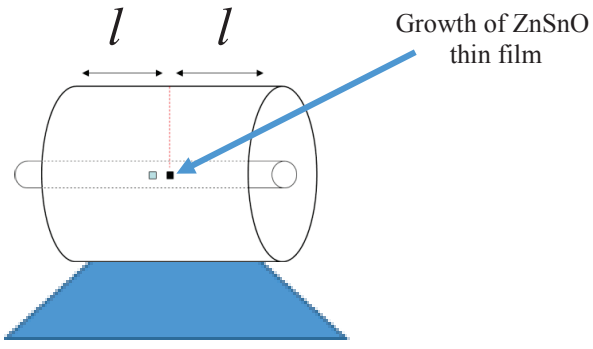


Figure 3.3. Schematic representation of tube furnace.

Especially for my thesis, the characterization of ZnSnO thin films depends on microstructure. So, in order to improve these properties, appropriate heat treatment steps of 450 ˚C anneal procedure is applied to have a control on grain size and morphology. Furthermore, it is aimed to get rid of stress inside the ZnSnO thin film samples.

## 3.2. Characterization Techniques

A wide variety of characterization techniques are used to evaluate the material quality of the thin films. The structural properties of thin films are studied by scanning electron microscopy (SEM) and X-ray diffraction (XRD). Composition measurements are made by energy dispersive analysis of X-rays (EDX) equipped with SEM. The electrical properties of the materials are investigated by Four-point probe measurements. The optical properties of films are studied using transmission measurements. The focus of this section is to characterize different experimental methods and devices used in applications for understanding the properties of the ZTO thin film.

### 3.2.1. Profilometry

A profilometer is a surface contact instrument with a stylus that is scanned across the samples surface for measuring film thickness. As the surface is scanned, a three-dimensional height profile is constructed from data. While the stylus is moving, it measures small surface variations in vertical. For example, thickness image of ZTO sample is that it shows thickness with a size around 100 nm, as seen in Figure 3.4.

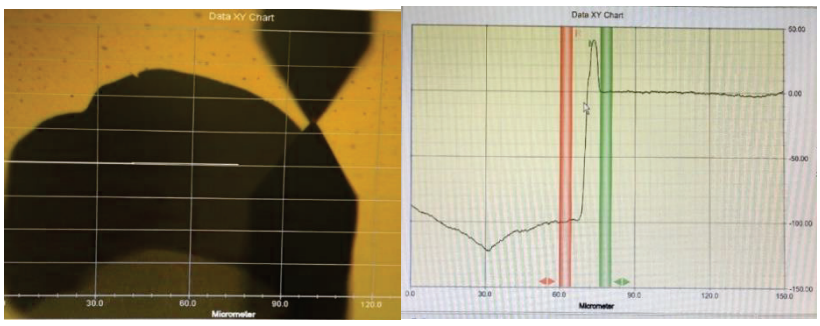


Figure 3.4. Thickness profile analysis of ZnSnO thin film.

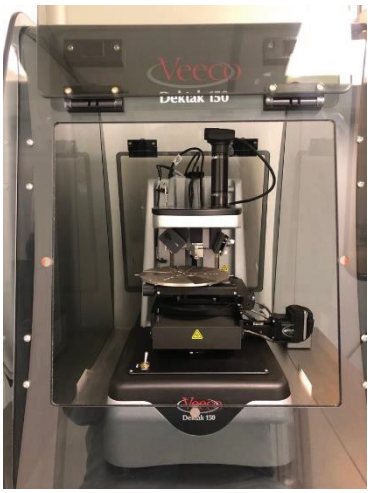


Figure 3.5. The picture of profilometer.

All ZTO thin films thicknesses that we used in this thesis were measured using a Veeco DEKTAK 150 profilometer. Illustration of working principle is a stylus profilometer in Figure 3.5. As the stylus is moved horizontally, the substrate will follow the surface of sample. The ZTO film thickness can be determined, by measuring the vertical movement of stylus.

### 3.2.2. Four-Point Probe

The four-point probe is a commonly used the technique to measure the semiconductor resistivity. It is an absolute measurement without recourse to calibrated standards and is sometimes used to provide standards for other resistivity measurements.


Figure 3.6. The picture of four-point probe.

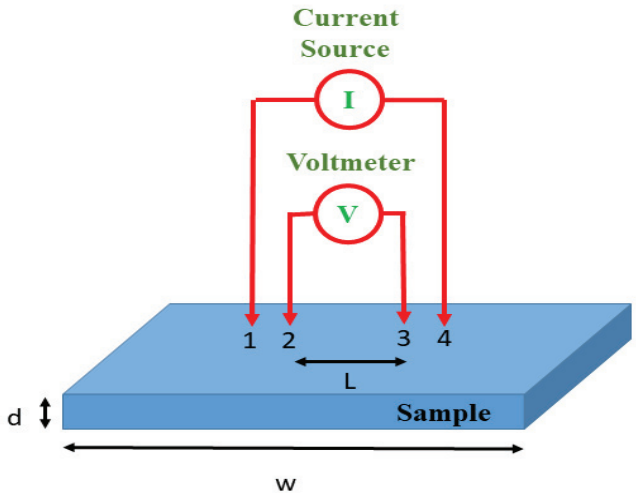


Figure 3.7. Schematic view of the four-point probe used in measuring resistivity.

In this method, the electrical contacts between setup and sample surface are four evenly spaced metal probes which are placed in a straight line, as depicted in Figure 3.6. In common type, an ammeter measures a current that passed through the sample. At the same time, a voltmeter measures a voltage of *V* produced across the inner part of the material. The picture of the four probe method was shown in Figure 3.7. It is seen that by applying current I between terminal 1 and 4 (outer terminals in the figure) and measuring voltage V across terminal 2 and 3 (inner terminals) one can calculate sheet resistance ($R_{Sh}$) of the film using following equation. Also, when the distance between the probes is far greater than the film thickness, the resistivity of the thin film can be calculated from equation. (Schroder 2005).

$$\rho = \frac{\pi d}{\ln(2)} \frac{V}{I} = R_{sh} d \qquad (3.1)$$

where $\rho$ is resistivity in Ω m, $d$ is ZTO film thickness in $m$, $R_{sh}$ is sheet resistance in Ω/square, width *(w)* and height *(t)*, $V$ is measured voltage over two inner probes, $I$ is the current that is supplied to the outer probes and the distance between two inner contacts of voltmeter probe is $L$ (Schroder 2005).The sheet resistance $(R_{sh})$ of sputtered conductivity of thin film on SLG such as ZTO thin films is used to measure by four-point probe system which is from using a Keithley 2425 instrument. On the other hand, the measured values of sheet resistance together with values of thickness of ZTO thin films obtained that can be used to calculate resistivity.

### 3.2.3. Spectrophotometry

A spectrophotometer is employed that reflection and transmission analysis of materials as a function of wavelength. In order to obtain the optical transmittance and the reflectance as a function of wavelength, a monochromatic light beam is used. Especially, spectrophotometer can be determined, dependently the control or calibration, so how much through calculations can be observed wavelengths of the samples. In my thesis, the optical required specification of ZTO thin film has been investigated via a PerkinElmer Lambda 950 UV/VIS/NIR portable spectrophotometer which includes wavelengths between 200 and 2600 nm.

### 3.2.4. Scanning Electron Microscopy (SEM)

Scanning Electron Microscopy (SEM) is an effective method to image between the morphology of thin films and the interfaces thin film layers. SEM resolves details one to two order orders of magnitude smaller than those analysable with optical microscopy. SEM analysis is used that creates an image of a small surface of thin films by firing a high-intensity beam of electrons at sample surface and scanning it in a zig-zag type pattern.SEM offered an insight into two dimensional and three-dimensional imaging of microstructure, chemical composition, crystallography and electronic properties (Egerton 2016). In this thesis, FEI-Quanta FEG 250 SEM by operating voltage in 20 k V was utilized to feature ZTO thin films and in order to be of opinion about the surface morphology and the existence of undesired phases aslope on ZTO thin film surfaces. Energy dispersive X-ray spectroscopy (EDX) diagnostics are commonly incorporated in scanning electron microscope setups since EDX measurements utilize an electron beam which is focused onto the investigated sample.

### 3.2.5. X-ray Diffraction (XRD)

X-ray diffraction (XRD) is a powerful technique that can be used to identify the atomic and molecular structure of a crystal, the crystalline phases that are present in a material. Analysis of XRD is applied by a collimated beam of X-rays of wavelength typically between 0.7-2 Å incidents on the sample surface. The wavelength of X-rays is

comparable with spacing between atoms. The beam is radiated by crystalline phases in sample according to Bragg's Law as shown in equation (Bragg 1913) :

$$n\lambda = 2dsin\theta \tag{3.2}$$

where $n$ is an integer, $\lambda$ is the photon wave length, $d$ is the distance between the parallel lattice planes, $\theta$ is the angle between the lattice plane and the incident radiation. The microstructural properties of ZTO thin films are analysed by XRD measurements performed in a Phillips X' Pert Pro X-ray diffractometer with CuKα radiation *($\lambda$=1.5406 Å*) under grazing incidence diffraction mode at a scanning rate of 0.016°/s in the *2$\theta$* range 20°–70°. As a reference, the stored database results of comparing have given.

### 3.2.6. Raman Spectroscopy

In 1928, Raman spectroscopy depends on Raman influence initial found by Raman (Klaassen and Hes 1986). It is described that can detect both inorganic and organic species and evaluate crystallinity of solids. In order to problem-solve in material, the susceptibility of crystal structure is one of the most important for Raman spectroscopy. For example, different Raman shifts give slightly different crystal orientations. The small amount of radiation energy is scattered when a beam of light is passed through a transparent substance. If monochromatic radiation is used, scattered energy will occur almost completely of radiation of incident frequency (Rayleigh scattering), but in addition, certain discrete frequencies above and below that of incident beam will be scattered. This extra inelastic scattering component is intended to as Raman scattering (I. W. Chiang et al. 2001). The analysis of the Raman shift can provide information about the chemical composition, molecular structure, and intermolecular interactions of the sample. While Raman studies were performing, Micro Raman-spectroscopy (S&I Mono Vista Raman System, 0.750 mm Imaging Triple Grating Monochrometer) used with excitation wavelength of 514.5 nm Ion-$Ar^+$ laser with 25mW power for ZTO thin films were taking with 600 gratings and 100x objective and using Si main mode at 521 $cm^{-1}$, calibration was done.

# CHAPTER 4

# RESULTS AND DISCUSSION

For the purpose of the ZTO films on polymer substrates for the characterization properties and good adhesion, the exhaustive work on these structural and electrical properties of the films is very important in my thesis. Also, to demonstrate that the advanced ZTO anodes are compatible with the OLED fabrication and to evaluate their performance. Coated thin films on SLG and polymers (PI and PET) were respectively characterized using many techniques. As results are that the deposition of method DC magnetron sputtering with the coated flexible ZTO/Ag/ZTO multilayer thin film electrodes will be promising indium-free that ıt is important to can replace conventional amorphous ITO electrodes. This chapter briefly outlines the thin film deposition methods used to deposit various ZnSnO thin films. The structural, morphological, characterization methods of thin films viz. profilometer, four-point probe, spectrophotometer, EDX, SEM, XRD, and Raman analyses are discussed. The optical and electrical methods to characterize semiconducting thin films are also discussed.

## 4.1 Sheet Resistance and Optical Transmission Measurements

Experimental stages can be divided into two parts. These parts consist of thin-film growth process including the experimental details such as ZnSnO thin films using ZT target and ZTO/Ag/ZTO thin films using ZTO target, respectively. Besides, the result of these experimental stages has been suggested the growth of ZnSnO thin films and ZTO/Ag/ZTO multilayer thin film electrodes like Profilometry, four-point probe, spectrophotometry.

In this part of my thesis, discussion on resistance and optical transmission measurements of the coated ZnSnO thin films and ZTO/Ag/ZTO multilayer thin film electrodes have been presented. Thus, the expected result of our experimental procedures is that, the surface resistance will be especially decreased from M Ω/□ to Ω/□ in addition to the highest transmittance in the visible region.

### 4.1.1 Growth Process of ZnSnO Thin Films Using ZT Target

Experimental studies are chosen to measure up the results of ZTO thin film growth with $Zn_2Sn$ (ZT) target under vacuum together with various parameters. For this purpose, $Zn_2Sn$ target material which has the formation 52% Zn and 48% Sn is grown on SLG substrate (1mm) at room temperature or at certain temperatures by using DC magnetron sputtering method. After the vacuum chamber was backfilled with flow rate of 30.0 sccm argon, pre-sputtering was made for 5 min to eliminate the waste surfaces of ZT target, and then shutter was opened. This some process is always done at every stage of experimental study. Finally, transmittance values in all measurements were used to measure at 550 nm is the SLG 91.6%, PI 73.1% and PET 59.2%.

Table 4.1. Sheet resistance, film thickness and transmittance for 450 °C-60 min annealed ZTO/SLG thin films obtained in various oxygen quantities.

| | Target-substrate distance (cm) | Deposition Time (min) | Ar/$O_2$ (sccm) | Thickness (nm) | Sheet Resistance (Ω/□) | Transmittance at 550 nm (%) |
|---|---|---|---|---|---|---|
| **Empty-SLG** | 0 | 0 | 0 | 0 | 0 | 91.6 |
| **ZT-01** | **7** | **5** | **30.0/5.0** | **72.0** | **5.98 k** | **73.3** |
| **ZT-02** | 7 | 5 | 30.0/7.5 | 70.3 | 14.0 k | 76.9 |
| **ZT-03** | 7 | 5 | 30.0/10.0 | 69.6 | 1.0 M | 77.8 |
| **ZT-04** | 7 | 5 | 30.0/12.5 | 58.8 | 5.0 M | 78.2 |

At the first stage of experimental procedures, during deposition applied power was constant, with increasing amount of oxygen ZTO thin films are coated on SLG substrates. The gas flow rate of Argon was sustained at 30.0 sccm while the gas flow rate of oxygen kept at 5.0 sccm, 7.5 sccm, 10.0 sccm and 12.5 sccm for these thin films, respectively. The sputtering power was kept at 15 Watt (W). Target-substrate distance was kept at 7.0 cm. The growth conditions were carried out at a DC power of 15 W (watt), deposition time of 5 min, base pressure of $2.0 \times 10^{-6}$ Torr. In order to induce their crystallization, the subsequent annealing process was carried out at 450 ˚C in an oxygen atmosphere for 60 minutes. As seen in Table 4.1, ZTO/SLG thin films are acquired with different thicknesses. Sheet resistance and optical transmittance values at 550 nm are calculated as shown in Figure 4.1. Oxygen amount and film thickness of thin film with

the lowest sheet resistance is detected. These measurements evince that sputtering power was not affected by thin films electrical and optical characteristics distinctly. For this reason, it was found that the oxygen amount of films with the lowest sheet resistance was obtained at 5.0 sccm $O_2$ and the best film properties were reached at ZTO thin films thicknesses of about 70.0 nm. However, the different parameters were continued as sheet resistance value is to be lower.

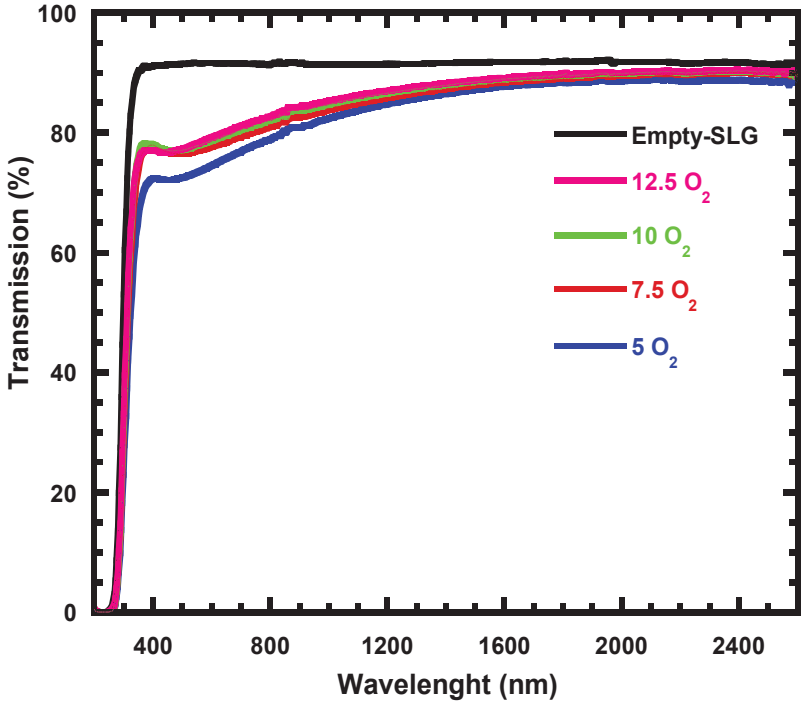


Figure 4.1. Optical transmissions graph for 450 °C-60 min annealed ZTO/SLG thin films obtained in various oxygen quantities.

At the second stage of experimental procedures, this deposition were applied at the DC power is 15 W, the gas flow rate is 30.0 sccm Ar and the target-substrate distance is 8.5 cm. Evidence from the literature suggests that the knowledge regarding sheet resistance in thin film will be decreased (Turkoglu et al. 2018). Therefore, we addressed that stress on thin films could be considerably diminished by the rotating sample holder during the deposition of thin films. As shows in Table 4.2, the upright interval from the target to substrate holder was increased from 7.0 to 8.5 cm. Moreover, the sheet resistances of the thin films are strongly related to the amount of oxygen vacancies and microstructure. Especially, the expected result of our experimental procedures was that the surface resistance decreased from kΩ/□ to Ω/□, so target-substrate distance was once again changed back to 7.0 cm. The increased target-substrate distance has not decreased

sheet resistance, but it has increased the optical transmittance at 550 nm was observed in the visible. However, the graph indicates that the increase in the optical transmittance is not complemented by the decrease in sheet resistance region, as seen in Figure 4.2.

Table 4.2. Sheet resistance, film thickness, and transmittance for ZTO/SLG thin films obtained in increasing target-substrate distance.

| | Target substrate distance (cm) | Ar/$O_2$ (sccm) | Deposition Time (min) | Thickness (nm) | Sheet Resistance (Ω/□) | Transmittance at 550 nm (%) |
|---|---|---|---|---|---|---|
| **Empty-SLG** | 0 | 0 | 0 | 0 | 0 | 91.6 |
| **ZT-05** | 8.5 | 30.0/12.5 | 5 | 50.0 | 7.0 M | 83.2 |
| **ZT-06** | 8.5 | 30.0/12.5 | 10 | 72.0 | 2.0 M | 77.2 |
| **ZT-07** | **8.5** | **30.0/7.5** | **10** | **70.3** | **9.0 k** | **77.5** |

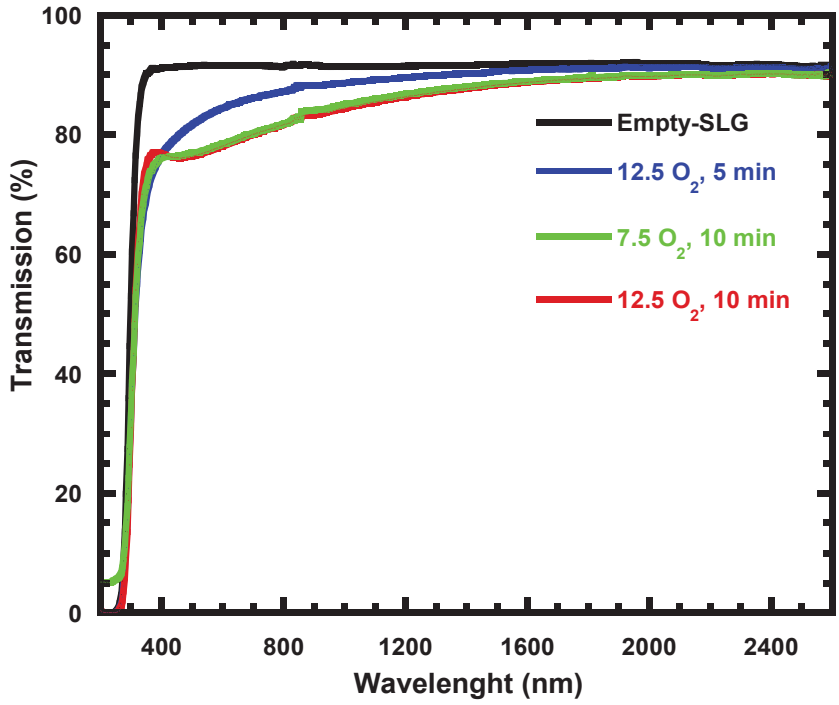


Figure 4.2. Optical transmissions graph for the increased target-substrate distance.

At the third stage of experimental procedures were enforced at DC power of 15 W, gas flow rate of 30.0 sccm Ar and 7.5 sccm $O_2$, target-substrate distance of 7 cm and deposition time of 10 min. Substrate temperatures were constantly kept at 100° C and 270° C, and surface temperature of SLG substrate was monitored by thermocouple and controlled by heater during deposition. Furthermore, the coated ZTO thin films have

decreased sheet resistance of this film homogeneously when the substrate temperature has increased as shown in Table 4.3.

Table 4.3. Sheet resistance, film thickness, and transmittance for ZTO/SLG thin films obtained in rising the substrate temperatures.

| | Target substrate distance (cm) | $O_2$ (sccm) | Deposition Time (min) | Substrate Temp. (°C) | Thickness (nm) | Sheet Resistance (Ω/□) | Transmittance at 550 nm (%) |
|---|---|---|---|---|---|---|---|
| **Empty-SLG** | 0 | 0 | 0 | 0 | 0 | 0 | 91.6 |
| **ZT-16** | 7 | 7.5 | 10 | 270 | 67.5 | 1.0 k | 81.9 |
| **ZT-18** | **7** | **7.5** | **10** | **100** | **87.5** | **35.0 k** | **84.5** |

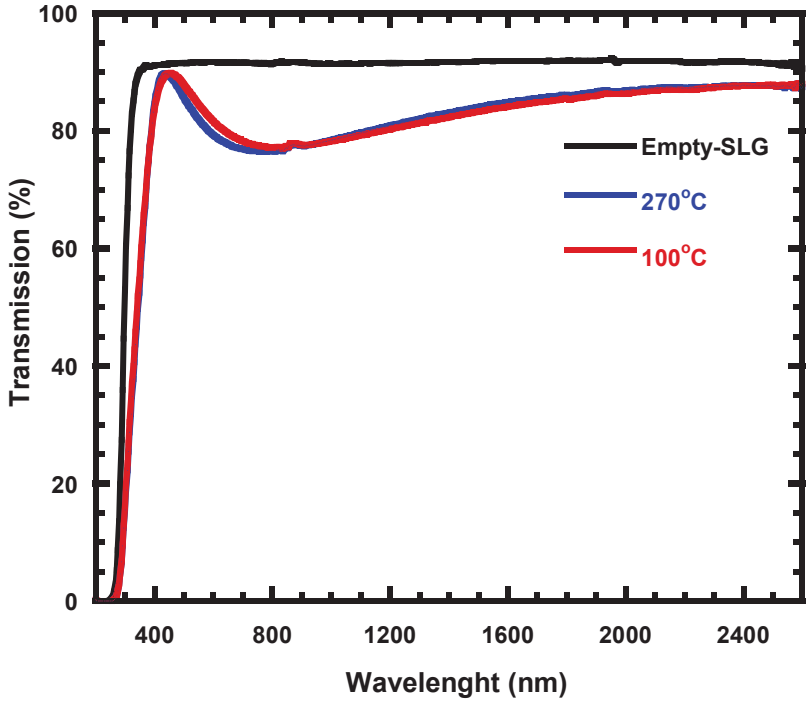


Figure 4.3. Optical transmissions spectra according to the substrate temperatures.

ZTO thin film observed to increase the optical transmission in the visible region as illustrates in Figure 4.3. The expected result of our experimental procedures is that the sheet resistance decreased at least 5.98 to 1.0 kΩ/□, we have seen that it was found the optical transmittance of 81.9% at the substrate temperature of 270 °C. In the visible range, the transmittance of the ZTO/SLG sample is observed to be lower than that of the bare SLG substrate however the variation is not substantial.

At the fourth stage of experimental procedures, in order to achieve dates on the reduction of internal pressure, the difference of gas flow $Ar/O_2$ ratios was constant

calibrated at the same temperature of 90 ºC. The different deposition time has enforced as 10 min and 20 min. For this reason, argon and oxygen values of 15.0/6.5 ratio have been reached the result of good conductivity in Table 4.4. Therefore, transmission has not changed against increase in the thickness of ZTO film in Figure 4.4.

Table 4.4. Sheet resistance, film thickness, and transmittance for ZTO/SLG thin films obtained in reducing of working pressure.

| | Target substrate distance (cm) | $Ar/O_2$ (sccm) | Deposition Time (min) | Thickness (nm) | Sheet Resistance (Ω/□) | Transmittance at 550 nm (%) |
|---|---|---|---|---|---|---|
| **Empty-SLG** | 0 | 0 | 0 | 0 | 0 | 91.6 |
| **ZT-27** | 7 | 20.0/8.5 | 10 | 40.0 | 7.6 k | 85.1 |
| **ZT-28** | **7** | **15.0/6.5** | **10** | **82.6** | **6.8 k** | **88.4** |
| **ZT-29** | 7 | 15.0/6.5 | 20 | 145.2 | 3.0 k | 88.3 |
| **ZT-30** | 7 | 20.0/8.5 | 20 | 115.9 | 19.0 k | 85.1 |

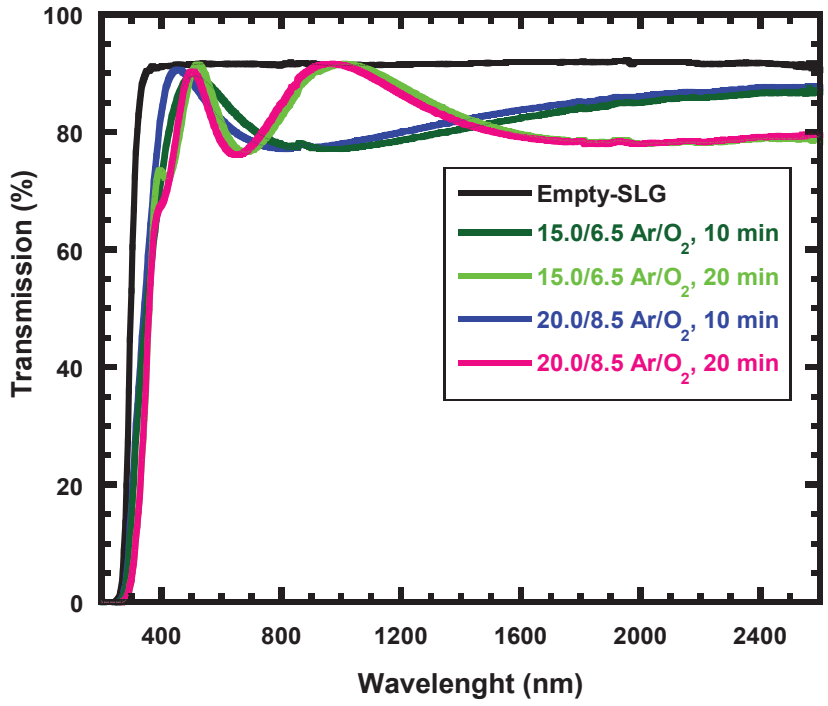


Figure 4.4. Optical transmission values dependently the working pressure.

At the final stage of experimental procedures were performed at the DC power is 15 W, the target-substrate distance is 7.0 cm, the gas flow rate is 15.0 sccm Ar and 5.5 sccm $O_2$, the deposition time of 10 min and the substrate temperature of 90 ºC as seen in Table 4.5. At the previous stage, sheet resistances and optical transmission values

depending on the reduction of working pressure so it has determined to desired at good resistivity and optical transmission. Sheet resistance and transmission values of 550 nm wavelength changing in from tables and graphs on shows decrease the amplitude of change in which it shows a fluctuation movement. In this study, the optical transmission values and the electrical resistance magnitudes of the coated ZTO thin film on SLG substrate that was found to vary depending on the thickness of peak values.

Table 4.5. Sheet resistance, film thickness, and transmittance for ZTO/SLG thin films obtained in making no substrate temperature.

| | Target substrate distance (cm) | Ar/$O_2$ (sccm) | Deposition Time (min) | Substrate Temp. (ºC) | Thickness (nm) | Sheet Resistance (Ω/□) | Transmittance at 550 nm (%) |
|---|---|---|---|---|---|---|---|
| **Empty-SLG** | 0 | 0 | 0 | 0 | 0 | 0 | 91.6 |
| **ZT-31** | **7** | **15.0/5.5** | **10** | **90** | **98.3** | **8.1 k** | **91.2** |
| **ZT-41** | 7 | 15.0/5.5 | 10 | 25 | 125.8 | 240.0 k | 86.1 |

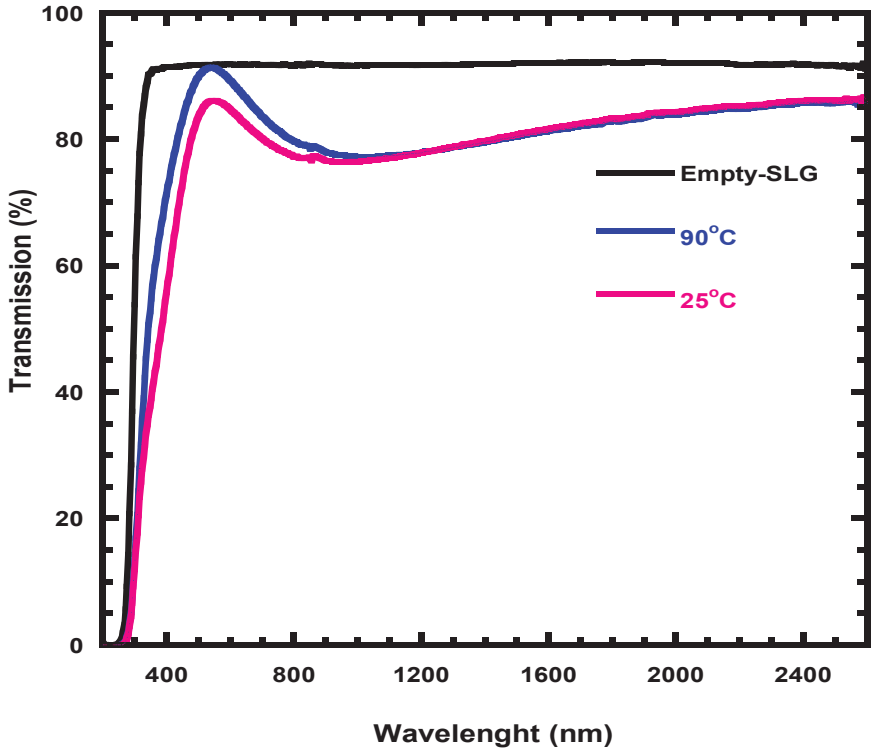


Figure 4.5. Optical transmissions graph for the result of ZT-31 thin films.

The final result, As shows in Figure 4.5, the optical transmittance value at 550 nm and the sheet resistance as growth ZT-31 thin film, 90.1%, and 8.1 kΩ/□ values are

that it has obtained as optimal values. Although the value obtained for the optical transmission value was good enough, the sheet resistance was approached to desired values. Thus, it is concluded that when the increased temperature was included in the films the sheet resistance of the films decreased. Consequently, for the growth of ZT-31 thin film, we succeed to achieve transmittance values closer to bare SLG substrates transmissivity.

### 4.1.2. Growth Process of ZTO/Ag/ZTO Thin Films Using ZTO Target

The focus of this growth process was coated ZTO, ZTO/Ag and ZTO/Ag/ZTO (ZAZ) multilayer thin film electrodes on SLG by DC magnetron sputtering using ZTO target at room temperature, respectively. And then, the same growth process was deposited thin film on polymers (PET and PI) by DC magnetron sputtering using ZTO target. The purpose of using soda lime glass before polymer substrate is using, ZAZ multilayer thin film electrodes were also grown on SLG to characterize in experimental details. Consequently, ZAZ electrodes, low resistivity, and high optical transmittance at room temperature could be achieving. The purpose of the performances of ZTO/Ag/ZTO multilayer electrodes indicate that ZAZ multilayers are promising as indium-free, transparent electrode substitutes for conventional ITO electrodes in cost-efficient OLEDs.

#### 4.1.2.1. Deposition of ZAZ Multilayer Thin Films on SLG

The experimental procedure at the first stage, ZTO thin films were deposited on SLG using ZTO target. In the best feature of the thin film could be coated by magnetron sputtering system at room temperature. These used growth parameters were applied via DC power of 15 W and target-substrate distance of 7.0 cm. Pre-sputtering was performed for 5 minutes before deposition process, then shutter was opened. Moreover, we have seen that when the gas flow of 30.0 sccm Ar and deposition time of 30 min values, the optical transmittance at 550 nm is the best values are given in Table 4.6. Optical transmittance spectra versus wavelength for growth and depending on the coated ZTO/SLG thin films, as seen in Figure 4.6. Especially, depending on the investigation of the effect of oxygen partial pressure and deposition time on the sheet

resistance and the optical properties of ZTO/SLG thin films have been realized in the experimental process. The decrease of the optical transmission while the argon gas flow rate increases both 30.0 sccm to 60.0 sccm is obtained since when excessive argon was included in the films the working pressure together with the sheet resistance of the films decreased. Especially, the investigation of the effect of deposition time and the gas flow rate on sheet resistance and optical properties of ZTO/SLG films have been realized.

Table 4.6. Film thickness and transmittance values of ZTO/SLG thin films.

| | Target substrate distance (cm) | Power ZTO (Watt) | Ar (sccm) | Deposition Time (min) | Thickness (nm) | Transmittance at 550 nm (%) |
|---|---|---|---|---|---|---|
| Empty-SLG | 0 | 0 | 0 | 0 | 0 | 91.6 |
| ZTO-1 | 7 | 15 | 30.0 | 10 | 50.3 | 83.1 |
| **ZTO-2** | **7** | **15** | **30.0** | **30** | **86.7** | **91.2** |
| ZTO-4 | 7 | 15 | 60.0 | 30 | 98.6 | 90.4 |

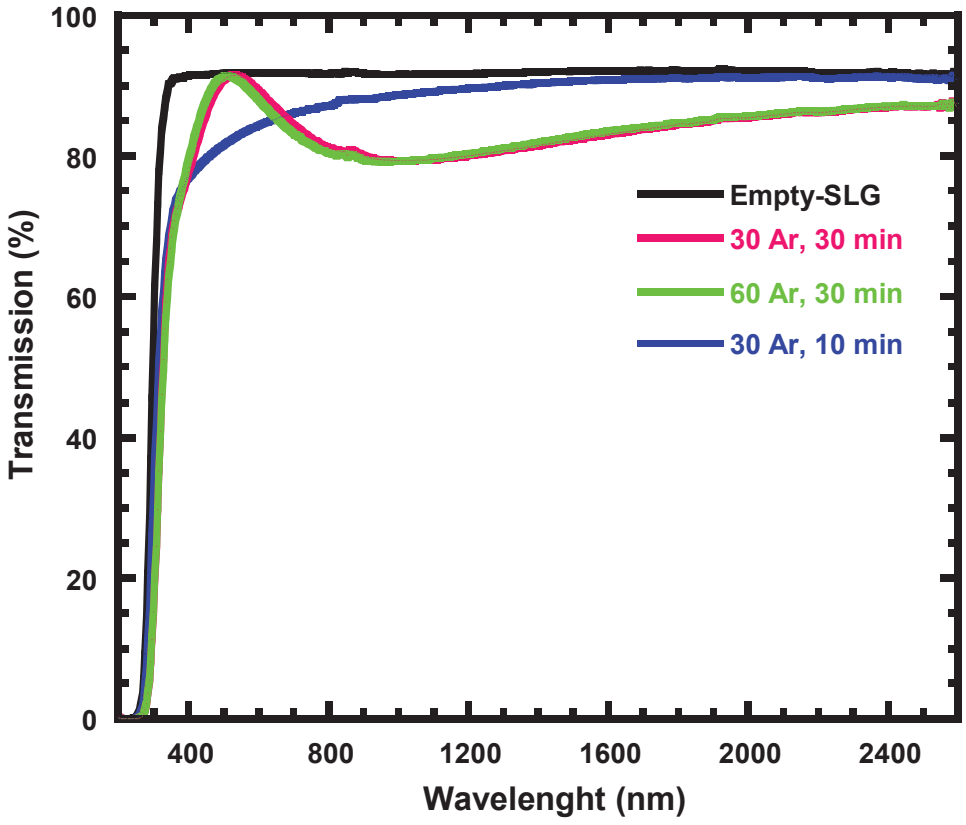


Figure 4.6. Optical transmissions graph for ZTO thin films on SLG substrate.

The profile analysis of Ag thickness, which was grown in SLG at 10s, 15s, 20s, 25s, 30s and 40s, respectively, we have seen that it was chosen as interlayer conductor

material as-growth of ZAZ multilayer thin film electrodes (Figure 4.7). Thus, the coating time of Ag films was decided to be 15s for measuring thin film whose thickness range of 10 to 20 nm in Table 4.7. Experimental studies in the literature of the ZTO/Ag/ZTO multilayer thin film electrode has showed decreased sheet resistance and resistivity with increasing Ag thickness. Especially, note that the result of the lowest resistivity is given the ZTO/Ag/ZTO multilayer using deposition time of 15 seconds. Although the thickness for obtaining Ag films by DC magnetron sputtering with various deposition time on SLG with a 12-nm-thick Ag layer showed the lowest resistivity, the Ag thickness was expected to be optimized at less than 12 nm, considering the low transparency of the thick Ag layer. In the present study, we succeed to achieve transmittance values closer to bare SLG substrates transmissivity.

Table 4.7. The thickness for obtaining Ag films by DC magnetron sputtering with various deposition time on SLG.

| **Thickness (nm)** | 10.9 | **12.4** | 14.3 | 14.2 | 16.2 | 17.9 |
|---|---|---|---|---|---|---|
| **Deposition Time (s)** | 10 | **15** | 20 | 25 | 30 | 40 |

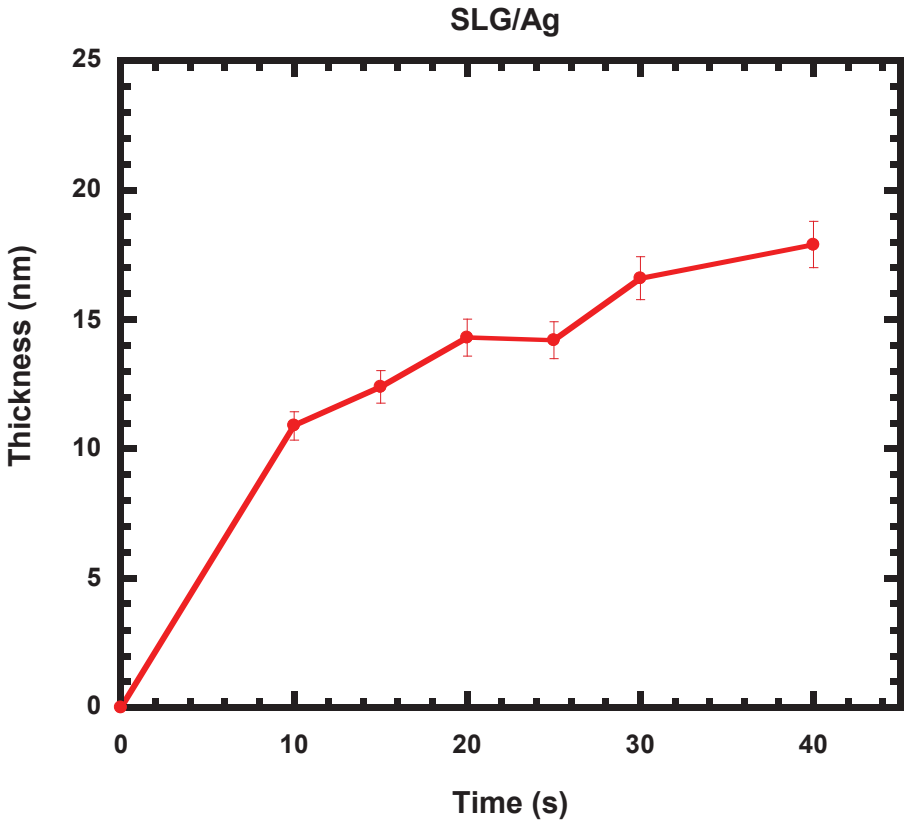


Figure 4.7. Thickness of Ag layer as a function of deposition time.

The experimental procedure at the second stage, the parameters of Ag thin film was performed power of 15 W, argon flow rate of 40.0 sccm, deposition time of 15 s and target-substrate distance of 7.0 cm. Therefore, Ag film was coated onto bottom ZTO thin film layer. Thus, ZTO-1/Ag thin film was grown on SLG using a specially designed dc magnetron sputtering method in room temperature at certain Ag dc powers under optimized ZTO film deposition conditions. For this reason, ZTO-1/Ag was reached the sheet resistance of 57.0 Ω/□ (Figure 4.8) and the optical transmittance 74.9% at 550 nm as shown in Table 4.8.

Table 4.8. Sheet resistance and transmittance of ZTO/Ag thin films on SLG.

| | Target substrate distance (cm) | Deposition Time Ag (s) | Power Ag (Watt) | Ar Ag (sccm) | Sheet Resistance (Ω/□) | Transmittance at 550 nm (%) |
|---|---|---|---|---|---|---|
| **Empty-SLG** | 0 | 0 | 0 | 0 | 0 | 91.6 |
| **ZTO-1/Ag** | 7 | 15 | 15 | 40.0 | 57.0 | 74.9 |
| **ZTO-2/Ag** | 7 | 15 | 15 | 40.0 | 58.2 | 70.1 |
| **ZTO-4/Ag** | **7** | **15** | **15** | **40.0** | **65.1** | **75.1** |

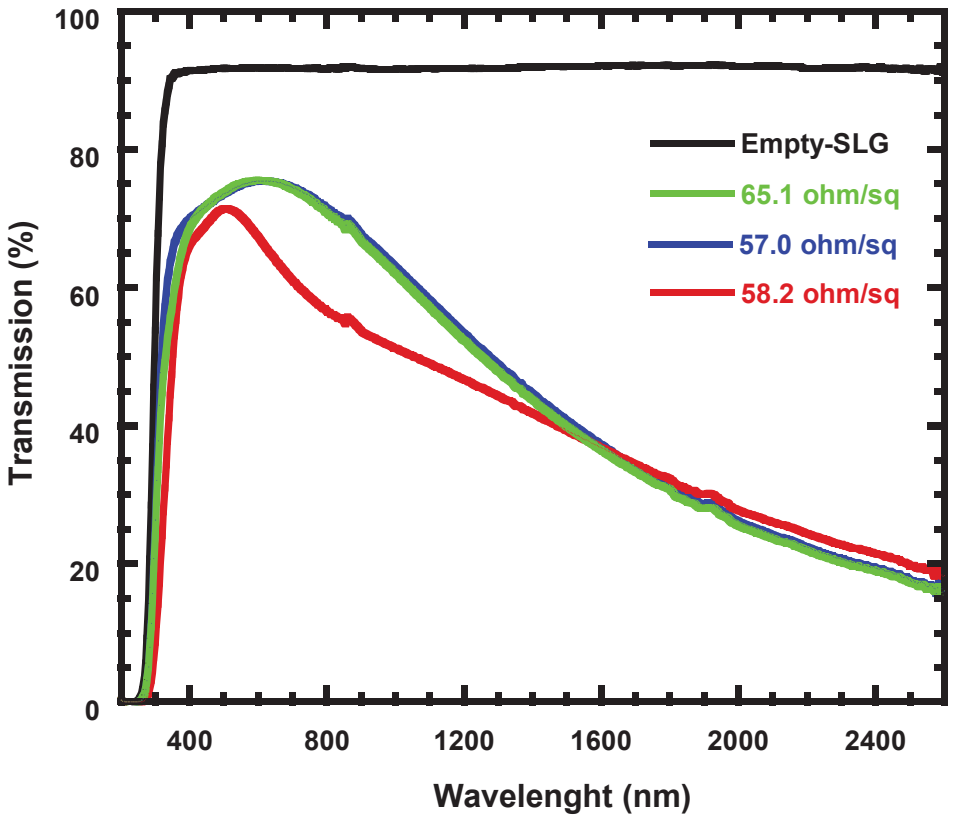


Figure 4.8. Optical transmissions graph for ZTO/Ag thin films on SLG substrate.

The experimental procedure at the third stage, after the ZTO/Ag thin films deposition, ZTO was coated on it with same parameters. ZTO/Ag thin film was coated on SLG by magnetron sputtering at the previous stage and then ZTO was coated with same parameters. As shown in Table 4.9 and Figure 4.9, the result of ZAZ-1 multilayer thin film electrode was achieved very well such as the minimum of sheet resistance is 2.6 Ω/□ and the maximum of the optical transmittance is 88.9% at 550 nm.

Table 4.9. Sheet resistance and transmittance values of ZAZ multilayer on SLG.

| | Target substrate distance (cm) | Power ZTO (Watt) | Deposition Time (min) | Ar (sccm) | Sheet Resistance (Ω/□) | Transmittance at 550 nm (%) |
|---|---|---|---|---|---|---|
| **Empty-SLG** | 0 | 0 | 0 | 0 | 0 | 91.6 |
| **ZAZ-1** | **7** | **15** | **10** | **30.0** | **12.6** | **88.9** |
| **ZAZ-2** | 7 | 15 | 30 | 30.0 | 3.0 k | 70.2 |
| **ZAZ-4** | 7 | 15 | 30 | 60.0 | 48.1 | 73.4 |

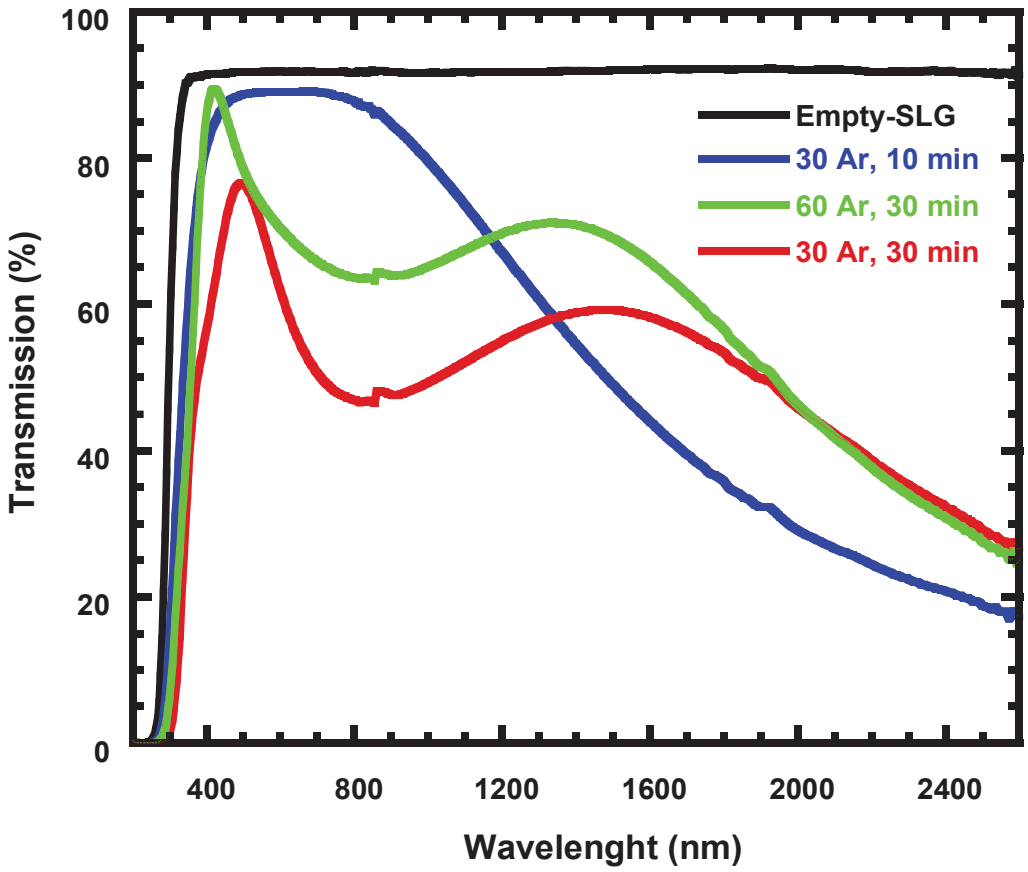


Figure 4.9. Optical transmissions graph for ZAZ multilayer on SLG.

### 4.1.2.2. Deposition of ZAZ Multilayer Thin Films on Polyimide

The experimental procedure at first stage, we had selected giver the best result of ZAZ-1 multilayer thin film electrode in the previous stage, which has known that the parameters were based on ZTO-1 thus The parameter of ZTO-1 has used in this stage. For this reason, ZTO thin films were grown on Polyimide (PI) via DC magnetron sputtering using of ZTO target at room temperature. this deposition was performed with 15 W, 30.0 sccm Ar, 10 min (deposition time) and target-substrate distance of 7.0 cm. As shown in Figure 4.10, the result of ZTO-1 multilayer thin film electrode was found to be the optical transmittance 66.9% at 550 nm. The experimental procedure at the second stage, after the ZTO-1 thin film deposition, Ag layer was deposited with same parameters before mentioned Ag (12.4 nm) layer.

Table 4.10 shows the sheet resistance of ZTO-1/Ag layer deposited on the PI substrate. In additional that the result of ZTO-1/Ag was found to be the optical transmittance 59.4% at 550 nm in additional to sheet resistance of 11.7 Ω/□. The experimental procedure at the third stage, in the previous stage, the Ag layer was sputtered on the bottom ZTO layer at the same thickness. The top ZTO layer was sputtered onto the Ag layers under the growth of the same conditions to those used to deposit the bottom ZTO layer. The result of the coated ZTO-1/Ag/ZTO-1 multilayer electrodes were found to be the optical transmittance 69.1% at 550 nm in additional to sheet resistance of 13.0 Ω/□.

Table 4 10. Sheet resistance and transmittance values of thin films on PI.

| | **Sheet Resistance (Ω/□)** | **Transmittance at 550 nm (%)** |
|---|---|---|
| **Empty-PI** | 0 | 73.1 |
| **ZTO-1/PI** | High resistance | 66.9 |
| **ZTO-1/Ag/PI** | 11.7 | 59.4 |
| **ZTO-1/Ag/ZTO-1/PI** | **13.0** | **69.1** |

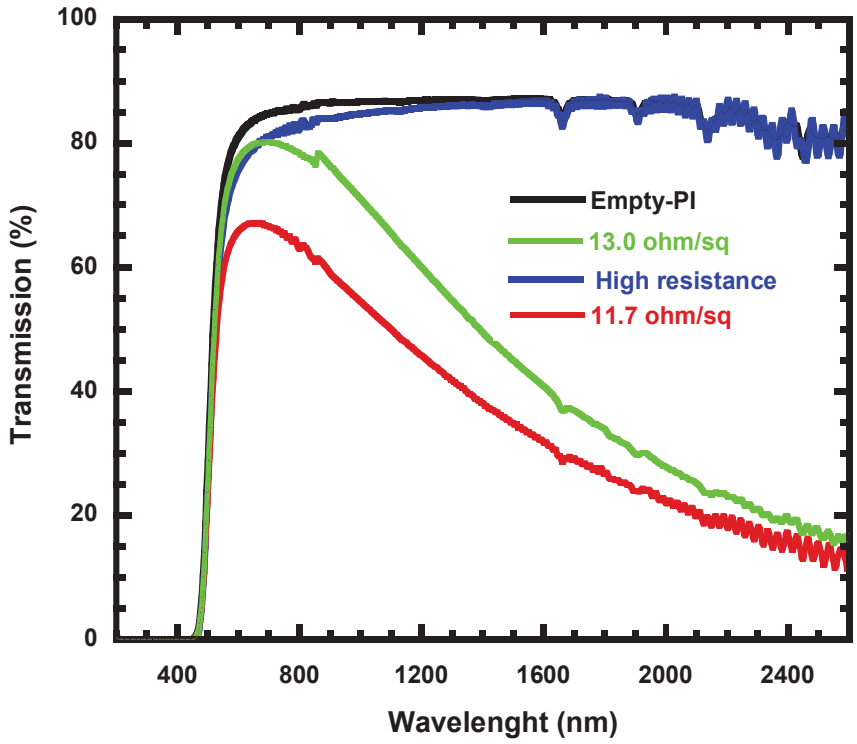


Figure 4.10. Optical transmissions graph for ZAZ multilayer on PI substrates.

### 4.1.2.3. Deposition of ZAZ Multilayer Thin Films on PET

The experimental procedure at the first stage, ZTO thin films were coated on PET films of 75 μm by dc magnetron sputtering using ZTO target. This deposition was performed with 15 W and target-substrate distance of 7.0 cm, 60.0 sccm Ar and 30 min values, the optical transmittance at 550 nm is the best value of ZTO-4 film, as seen in Table 4.11. Optical transmittance spectra versus wavelength depending on ZTO/PET thin films in Figure 4.11.

Table 4.11. Optical transmittances values of ZTO/PET thin films.

| | Target-substrate distance (cm) | Power ZTO (Watt) | Ar (sccm) | Deposition Time (min) | Transmittance at 550 nm (%) |
|---|---|---|---|---|---|
| **Empty-PET** | 0 | 0 | 0 | 0 | 59.2 |
| **ZTO-1** | 7 | 15 | 30.0 | 10 | 54.9 |
| **ZTO-2** | **7** | **15** | **30.0** | **30** | **62.9** |
| **ZTO-4** | 7 | 15 | 60.0 | 30 | 63.3 |

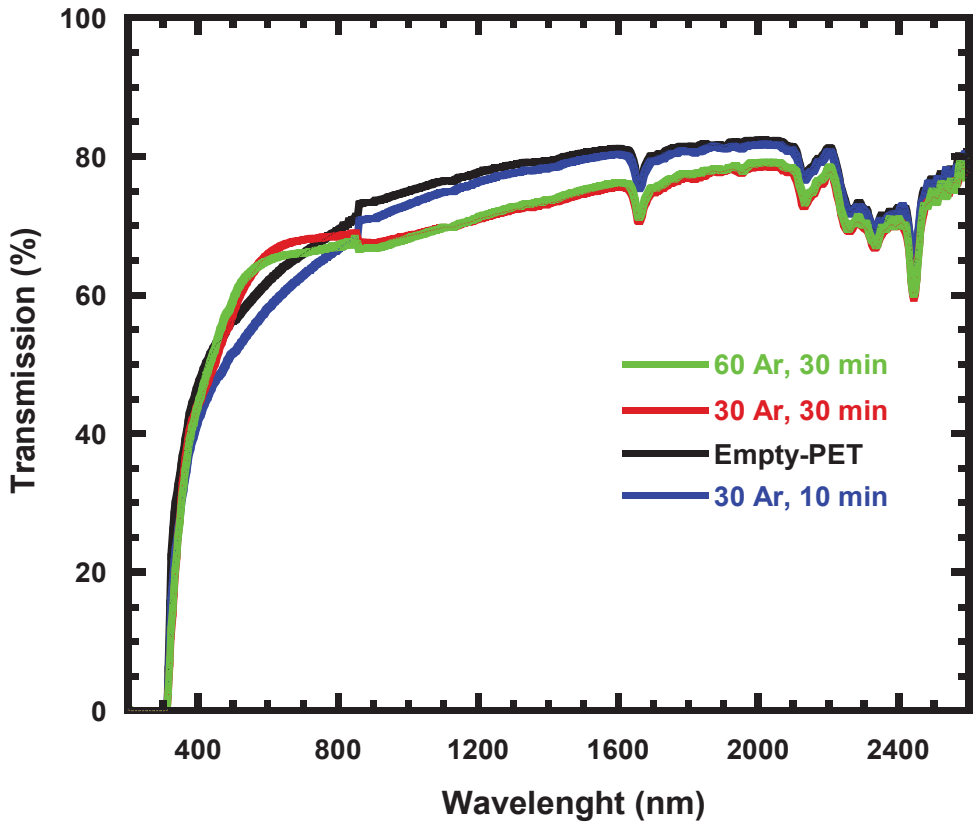


Figure 4.11. Optical transmissions graph for ZTO thin films on PET substrate.

The experimental procedure at the second stage, Ag layer was deposited with same parameters Ag layer after the ZTO-1 thin film deposition. The sheet resistances of ZTO-1/Ag layer deposited on the PET substrates are illustrated in Table 4.12. In Figure 4.12, the expected result of our experimental procedures was that ZTO-1/Ag was found as optical transmittance 54.1% at 550 nm.

Table 4.12. Sheet resistance and transmittance values of ZTO/Ag/PET films.

| | Target substrate distance (cm) | Deposition Time Ag (s) | Power Ag (Watt) | Ar Ag (sccm) | Sheet Resistance (Ω/□) | Transmittance at 550 nm (%) |
|---|---|---|---|---|---|---|
| **Empty-PET** | 0 | 0 | 0 | 0 | 0 | 59.2 |
| **ZTO-1/Ag** | 7 | 15 | 15 | 40.0 | 14.0 | 50.9 |
| **ZTO-2/Ag** | **7** | **15** | **15** | **40.0** | **10.8** | **54.1** |
| **ZTO-4/Ag** | 7 | 15 | 15 | 40.0 | 17.2 | 53.0 |

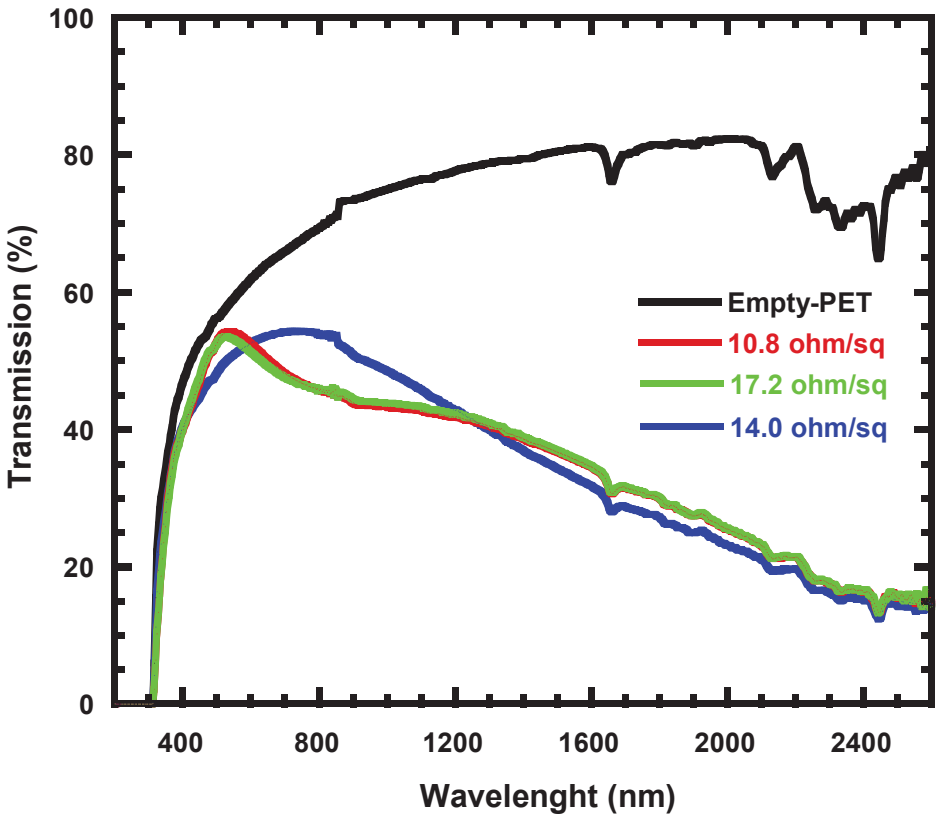


Figure 4.12. Optical transmissions graph for ZTO/Ag thin films on PET.

The experimental procedure at the third stage, Ag layer was coated on the bottom ZTO layer at the same thickness at the previous stage. As a consequence, the same thickness of the top ZTO layer was coated onto Ag layers under the growth of the same conditions to those used to deposit the bottom ZTO layer. As shown in Table 4.13 and Figure 4.13, the result of ZAZ-1 multilayer thin film electrode was achieved very well the sheet resistance of 20.8 Ω/□ and the optical transmittance of 62% at 550 nm.

Table 4.13. Sheet resistance and transmittance values of ZAZ/PET multilayer.

| | Target substrate distance (cm) | Power ZTO (Watt) | Ar (sccm) | Deposition Time (min) | Sheet Resistance (Ω/□) | Transmittance at 550 nm (%) |
|---|---|---|---|---|---|---|
| **Empty-PET** | 0 | 0 | 0 | 0 | 0 | 59.2 |
| **ZAZ-1** | **7** | **15** | **30.0** | **10** | **20.8** | **54.9** |
| **ZAZ-2** | 7 | 15 | 30.0 | 30 | 21.3 | 55.9 |
| **ZAZ-4** | 7 | 15 | 60.0 | 30 | 21.7 | 53.3 |

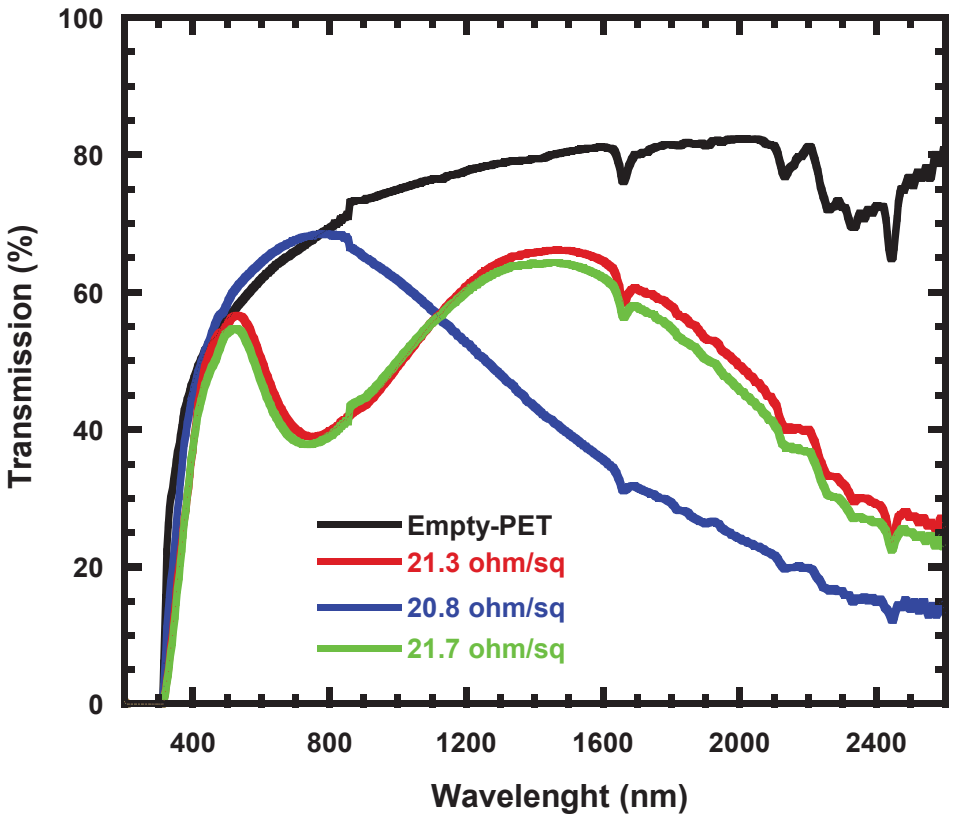


Figure 4.13. Optical transmissions depend on ZAZ multilayer on PET substrate.

## 4.2. SEM Analysis of Samples

Scanning electron microscopy (SEM) was used to define the morphology of homogeneous surface. SEM images of ZTO thin films are very smooth without defects such as cracks, pinholes, pores and protrusion under continuous DC magnetron sputtering. The smooth surface is so significant that anode layers can cause break down or short-circuit for flexible OLEDs. Composition of the thin films can be controlled with energy dispersive X-ray spectroscopy (EDX) unit of the SEM, as the Zn, Sn, O, and Ag can be detected. Also, another problem arises due to the low thickness of the thin films, which causes an electron beam to penetrate through the thin film easily and access the underlying SLG. Therefore, it was removed from used substrate information. SEM images and EDX results of ZT-31 thin film on SLG substrate was shown in Figure 4.14. It was shown uniform surface. Particle sizes almost the same O, Zn, Sn elements have respectively 87.98%, 7.27% and 4.74% atomic ratios. In still another analysis, SEM images and EDX results of ZTO/Ag (12.4 nm)/ZTO (ZAZ-1) multilayer thin film

electrode on SLG substrate was illustrated in Figure 4.15. It was shown uniform surface. Particle size almost the same O, Zn, Ag, Sn elements have respectively 82.19%, 13.65%, 1.15% and 3.01% atomic ratios. Despite both ZTO thin films and ZAZ multilayer thin film electrodes were produced from target with elemental analysis performed by EDS reveals that Zn-poorer thin films are obtained relative to the expected target composition, as seen in Figure 4.14 and 4.15.

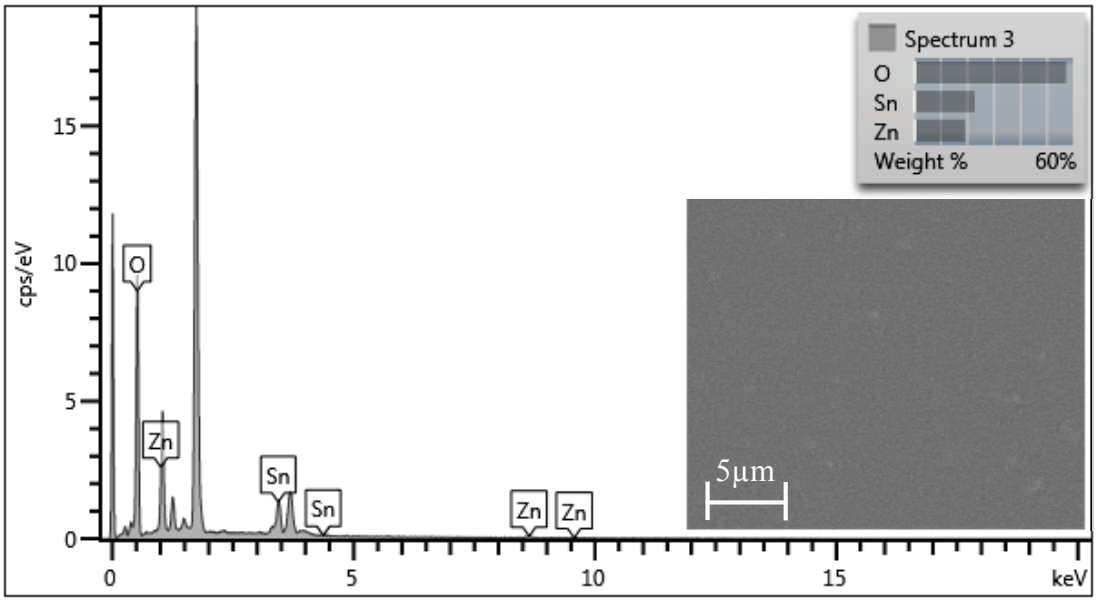


Figure 4.14. EDX result of ZT-31 film using $Zn_2Sn$ (ZT) target on SLG substrate

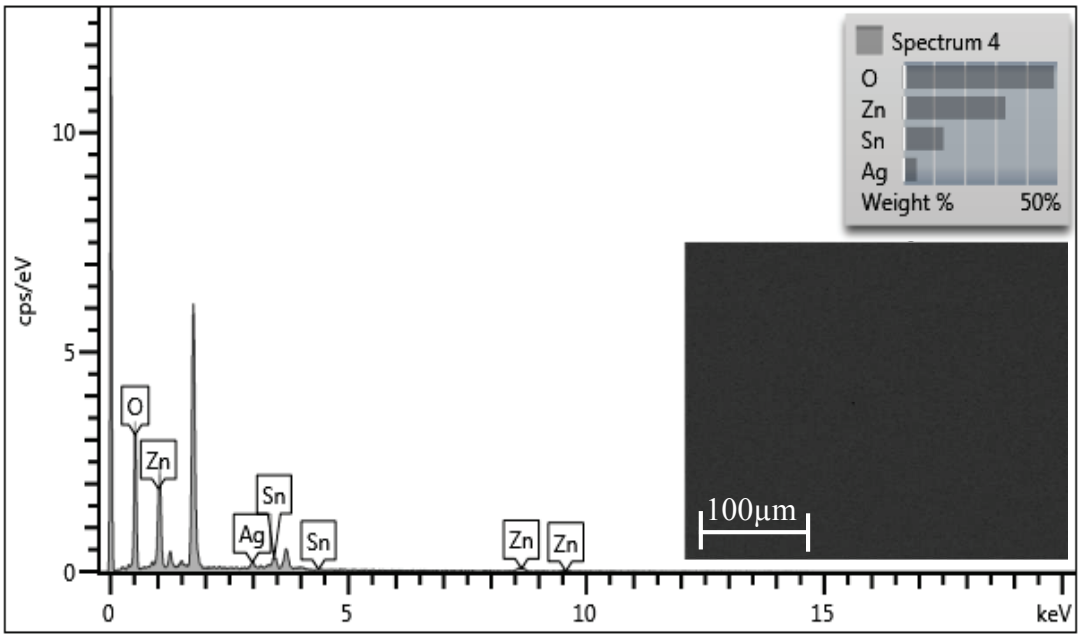


Figure 4.15. EDX result of ZAZ multilayer using ZnSnO (ZTO) target on SLG.

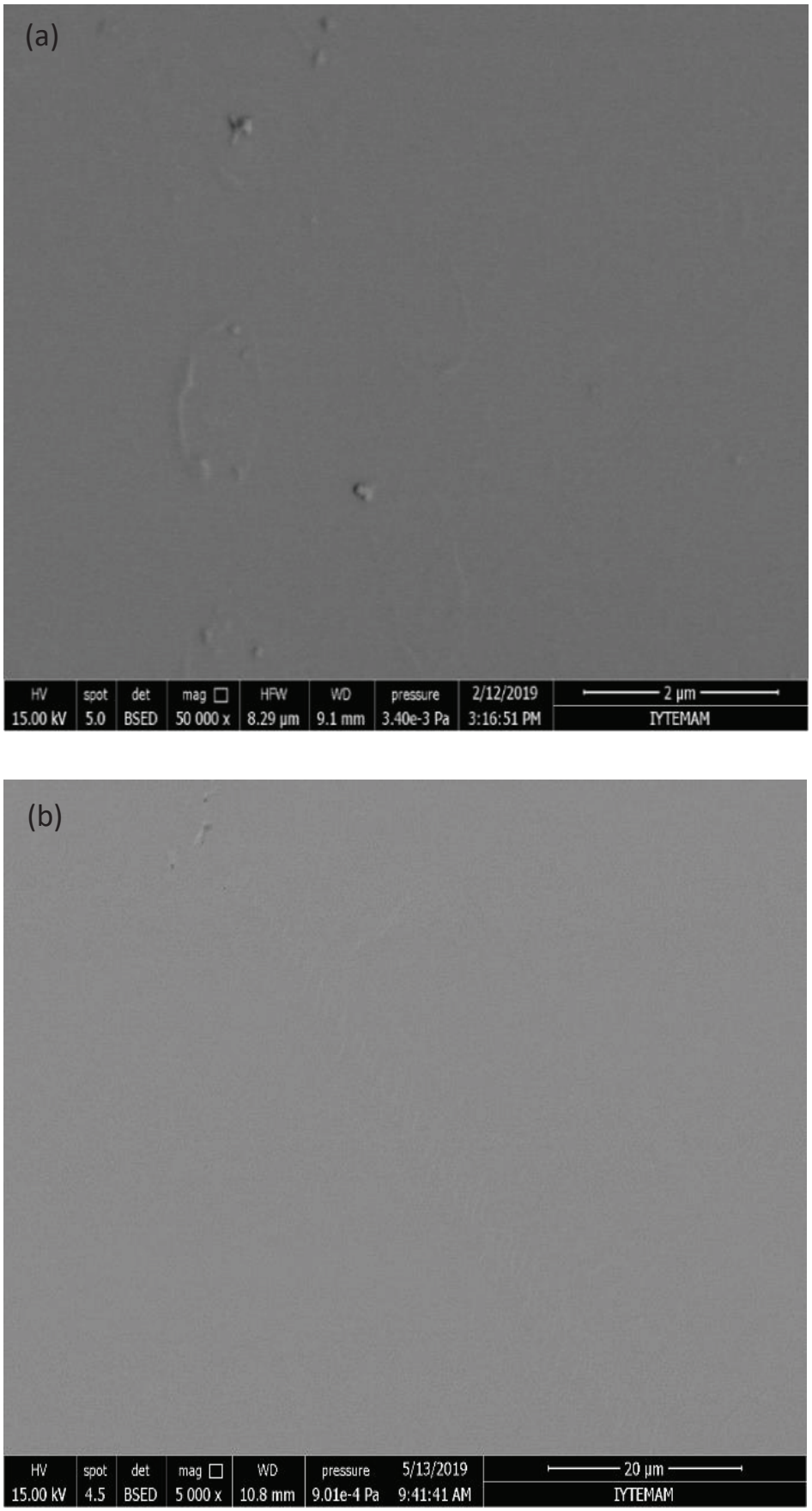


Figure 4.16. SEM images of (a) ZT-31 thin film (50000x magnification) (b) ZAZ-1/SLG multilayer thin film electrode (50000x magnification)

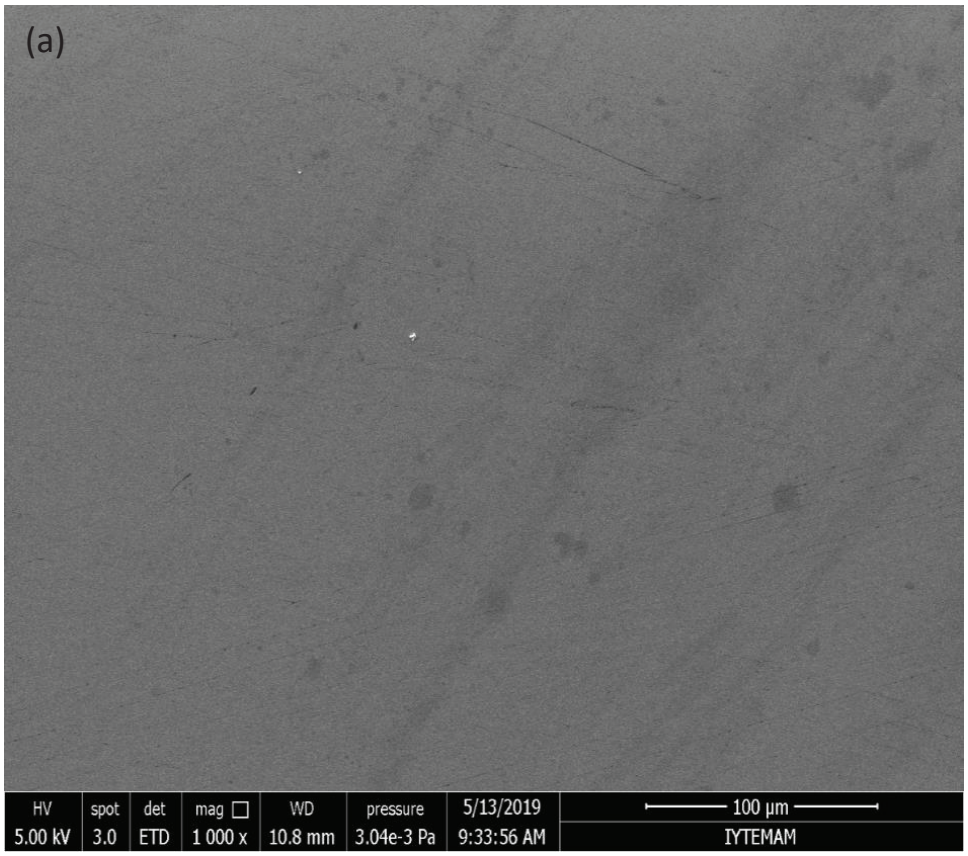


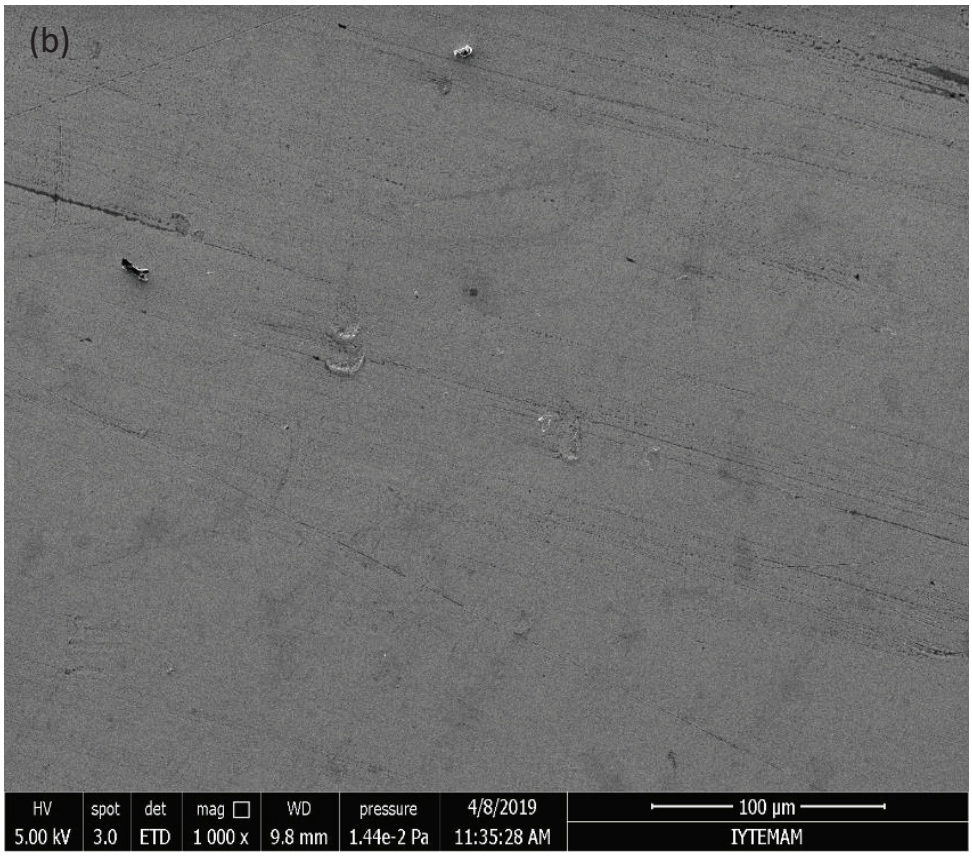


Figure 4.17. SEM images of (a) ZAZ-1/PI multilayer thin film electrode (1000x magnification) (b) ZAZ-1/PET thin film (1000x magnification)

SEM measurements of (a) ZT-31 thin film (50000x magnification) (b) ZAZ-1/SLG multilayer thin film electrode (50000x magnification), respectively. The ZTO thin films were deposited both ZT-31 thin film and ZAZ-1 multilayer thin film electrode on SLG by DC magnetron sputtering, as mentioned before (Figure 4.16). In additional to that Figure 4.17 is shown SEM measurements of (a) ZAZ-1/PI multilayer thin film electrode (b) ZAZ-1/PET multilayer thin film electrode. This results of the analysis are in good agreement with the literature results. SEM images ZAZ sample were given that thin films contain thickness with a size around 200 nm and ZT samples indicate that thin films contain thickness with a size around 100 nm. The flexible ZAZ-1 electrodes were continuously sputtered on polymers (PET and PI) substrates using a DC magnetron sputtering system at room temperature under optimized ZTO growth conditions. From the measurement of values, we determined that the flexible ZAZ-1/PI multilayer thin film electrode was deposited to be the sheet resistance of 13.0 Ω/□ and optical transmittance of 69.1% the optimized sample. In the same way, we determined that the flexible ZAZ-1/PET multilayer thin film electrode was deposited the sheet resistance of 20.8 Ω/□ and optical transmittance of 62.0% the optimized sample. Regardless of used polymers, the films exhibited surface morphology. At the optimized Ag thickness (12.4 nm), both the PI and PET substrates had smooth surface morphologies. All top ZTO layers in the flexible ZAZ-1 multilayer thin film electrodes exhibited very smooth and flat surface images, due to deposit at the low temperature of the polymer substrates, which is constant maintained by the water cooling process. As a consequence, these samples can be used to determine ZTO as an anode in OLED production.

## 4.3. XRD Analysis of Samples

X-ray diffraction (XRD) is a very considerable experimental technique in revealing the crystal structure of thin films. X-ray diffraction measurement could be determined the data involved the crystal structure of the films such as consist of unit cell parameters, defects, stresses, grain size, compositions, hardness, etc. The XRD plots of the ZTO film was grown on SLG and polymer substrate. Consequently, ZTO film was enlarged by dc magnetron sputtering deposition condition, dense and uniform structure was observed. However, the amorphous properties of some thin films have not completely disappeared. Our x-ray diffraction analysis for ZTO thin film and ZAZ-1 multilayer thin film electrode from TCO products established no crystalline

(amorphous) state of these glassy materials as seen in Figure 4.18 and 4.19. Furthermore, the broadband of weak diffraction was observed, peaking at around 2$\Theta$ 24.90° to 25.90°, without concomitance of any diffraction line assigned to crystalline forms. This distribution is characteristic of SnO-based oxide glasses studied for SnO-$SiO_2$ systems.

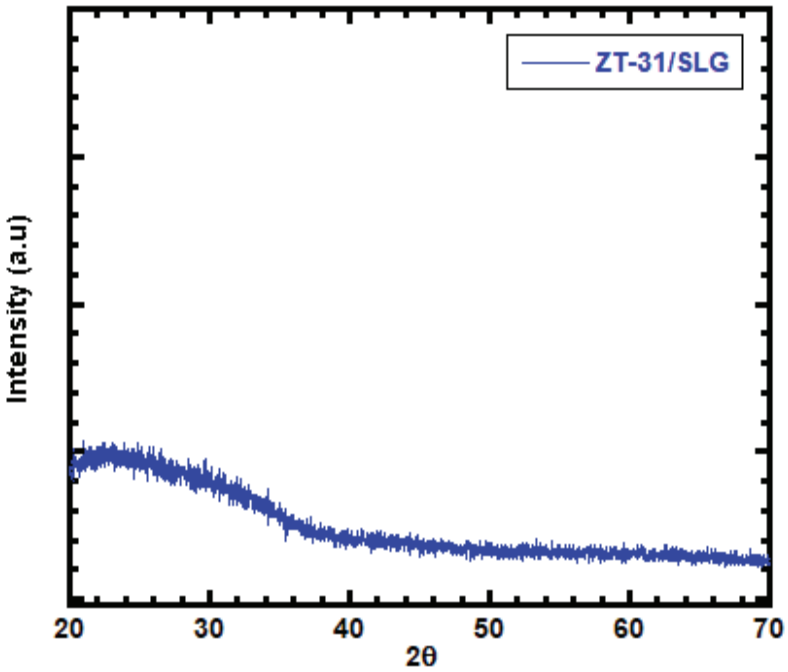


Figure 4.18. XRD patterns of ZT-31 thin film.

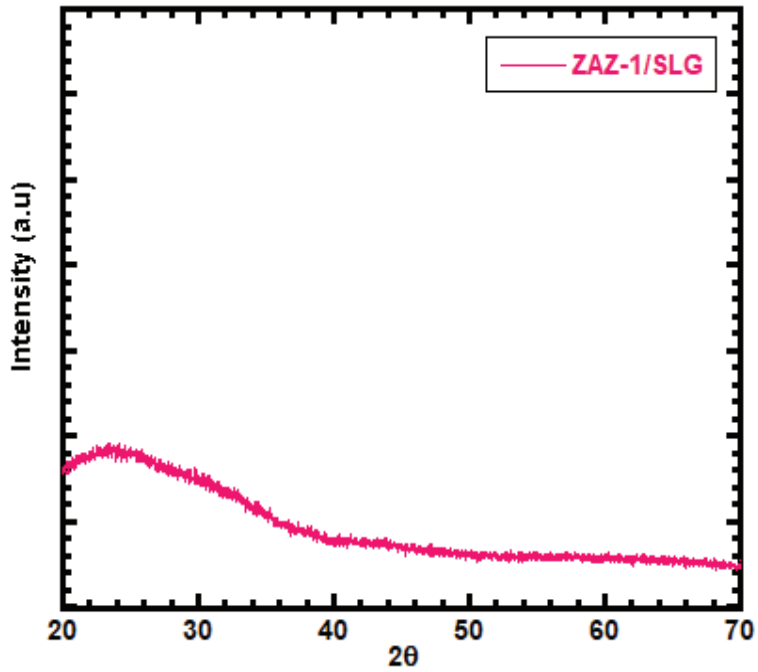


Figure 4.19. XRD patterns of ZAZ-1/SLG multilayer thin film.

The results of X-ray diffraction patterns of the pristine polyimide film are presented in Figure 4.20. It could be found that there are peaks at 20.2°, 26.5° and 38.2° which could be indexed as (110), (012) and (111) respectively. It can be inferred that the semi-crystalline structural pristine polyimide is still regularly ordered in certain degrees. X-ray diffraction pattern matches with the standard data card (JCPDS file No. 28-1486). As shown in Figure 4.21, the XRD scattering angles at 25.84°, 38.02°, 44.38° and 54.23° correspond to the (100), (111), (200), (241) crystal planes (hkl) respectively, reveals an orthorhombic phase of $ZnSnO_3$ (JCPDS 01-078-3428). Absence of any extra peaks indicates high purity of $ZnSnO_3$. The structure of ZTO films deposited on PET substrates, meanwhile, was hardly understood from XRD pattern, since the diffraction peaks of ZTO films are submerged in a very strong peak of the PET substrate. The peak intensities of planes increase with increasing sputtering pressure, indicating that the degree of preferential orientation toward these directions increases.

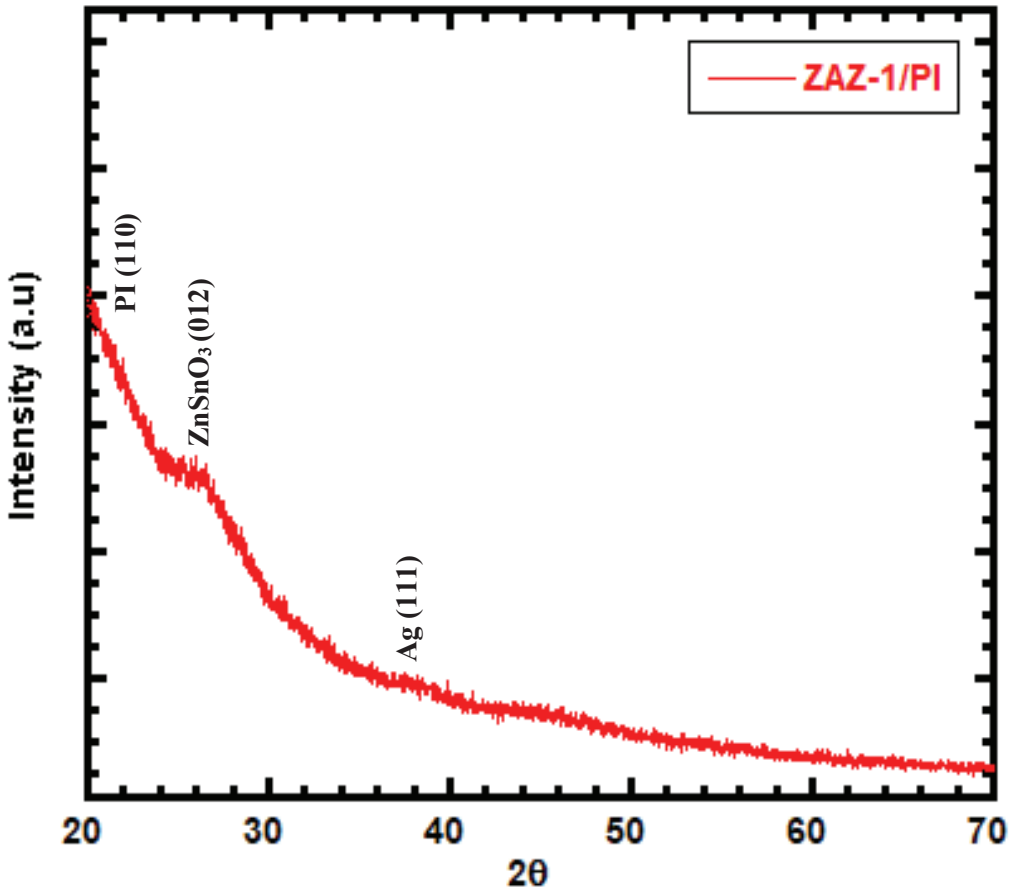


Figure 4.20. XRD patterns of ZAZ-1/PI multilayer thin film.

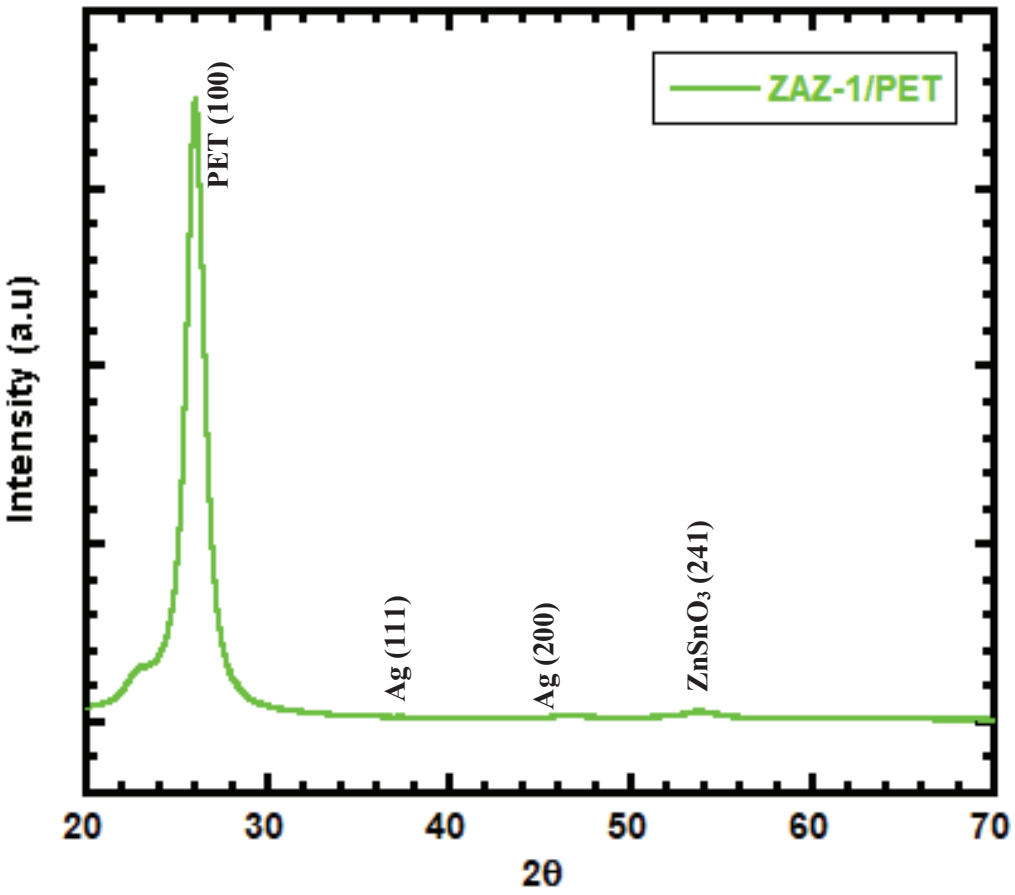


Figure 4.21. XRD patterns of ZAZ-1/PET multilayer thin film electrode.

## 4.4. Raman Analysis of ZT-31 Sample

Figure 4.22 is shown the Raman spectra of the coated ZTO thin film. Excitation in 514.5 nm wavelength with 600 gratings and 150 nm penetration depth for the coated ZT-31 film on SLG substrate was used to characterize this film. Under certain temperature Raman spectrum of the ZTO thin film was also measured. Furthermore, the Raman shift peaks at 559.80 $cm^{-1}$, 224.01 $cm^{-1}$ and 297.19 $cm^{-1}$ correspond to well-known ZTO Raman shift peaks appear here. Moreover, this peak at 778.14 $cm^{-1}$ was attributed to the first order Raman-active modes vibration modes of $SnO_2$ which are in agreement with previously reported theoretical studies (Saafi et al. 2016). These results are in good agreement with the results of Scott and other workers (Scott 1970). Such a result confirms spinel-structured ZTO crystals with a tiny concentration of impurities. Compared to other reports, the 559.80 $cm^{-1}$ peak here is broadened and split into two peaks at ~553 $cm^{-1}$ and ~607 $cm^{-1}$.

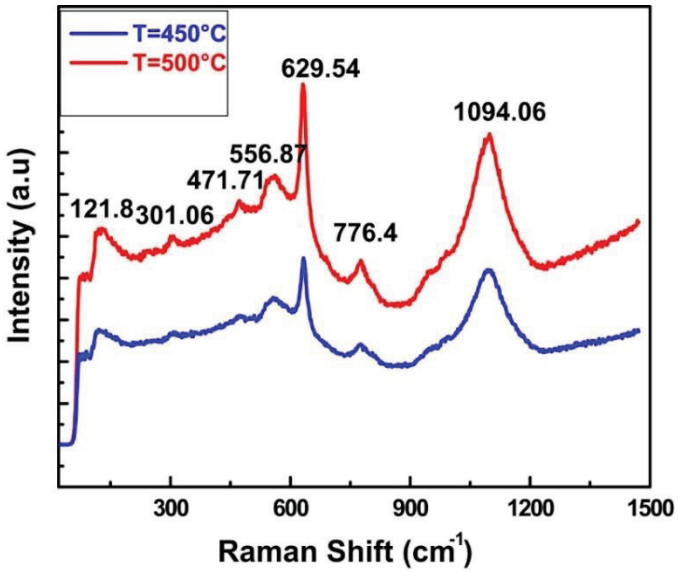


Figure 4.22. Raman spectra of $SnO_2$–$ZnSnO_3$ films obtained at room temperature. (Source: Saafi et al. 2016).

As a result of literature is that, we consider that such variation may be regarded as the size effect of thin films or the effect of oxygen and other defects (Anisotropy et al. 1970). Moreover, the peak at ~553 $cm^{-1}$ could be ascribed to vibrational modes of the vacancy related defect (Mereu et al. 2015). On the other hand, the signal at 559.80 $cm^{-1}$ is associated with $ZnSnO_3$. Finally, the peak observed at 1094.21 $cm^{-1}$ is due to glass substrate (Yahia et al. 2008).

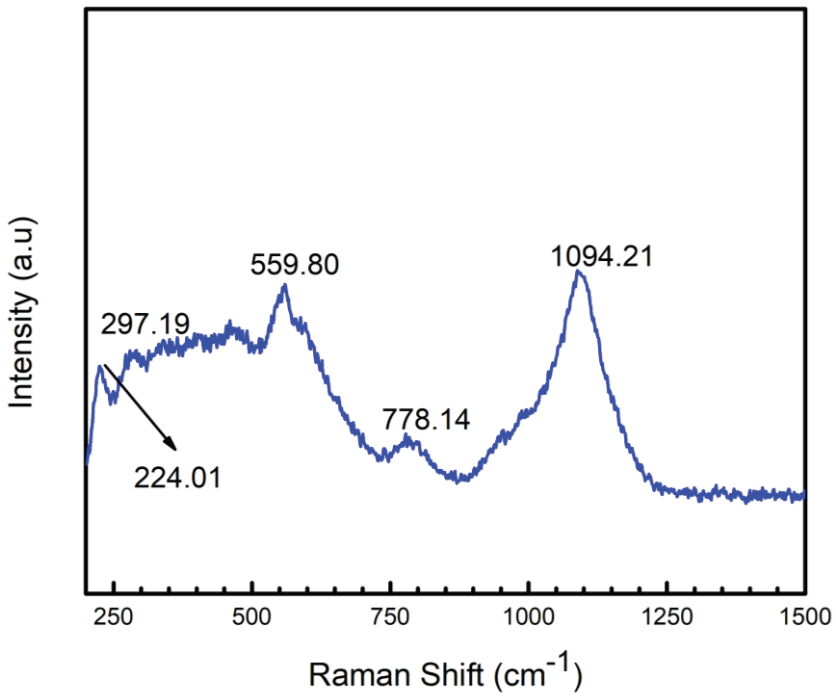


Figure 4.23. Raman spectra of ZT-31/SLG thin film.

# CHAPTER 5

# CONCLUSION

In my thesis, as the result of the zinc tin oxide (ZTO) films and ZTO/Ag/ZTO (ZAZ) multilayer thin film electrodes growth was presented in a number of different parameters of low sheet resistance and high optical transmittance. Transparent conductive ZTO thin films of low sheet resistance and high optical transmittance at 550 nm were coated on unheated substrates and certain substrate temperature with various oxygen gas flows using DC magnetron sputtering system. Hence, based on the obtained outcomes following remarks can be determined as follows:

To optimize conditions from the growth of ZnSnO thin films by ZT Target is the best parameters that it was performed at the DC power is 15 W, the target-substrate distance is 7.0 cm, the gas flow rate is 15.0 sccm Ar and 5.5 sccm $O_2$, the deposition time of 10 min and substrate temperature of 90.4 $^oC$. Consequently, the sheet resistance and the optical transmittance of ZTO thin films with a thickness of 98.3 nm were 8.1 kΩ/□ and 90.1%, respectively. Also, the sheet resistance of thin film has shown to decrease with increasing thickness of the ZTO thin film.

Knowing that the reason for the selection of Ag material from metals for interlayer conductive material was chosen to obtain ZAZ multilayer thin film electrodes with high conductivity and transmission. Moreover, the goal is to create ZAZ multilayer thin film electrodes by increasing Ag layer (12.4 nm) between two ZTO coatings (each layer 50 nm to 100 nm) to compare three different parameters for growth and development of ZAZ multilayer thin film electrodes. As a result, the sheet resistance of the upper layer ZTO can be decreased. In this way, the sheet resistance can so low much while optical transmission can increase. Furthermore, in order to compare the performance of the ZTO and ZAZ multilayer thin film electrodes as flexible and transparent anodes for OLEDs, we fabricated typical thin films on ZTO/PI, ZTO/PET, ZTO/SLG, ZAZ/PI, ZAZ/PET, and ZAZ/SLG.

After that, ZAZ/SLG multilayer thin film electrode was found to be the lowest sheet resistance of 12.6 Ω/□ and the optical transmittance of 88.9%. Then, ZAZ/PI multilayer thin film electrode was found to be the lowest sheet resistance of 13.0 Ω/□

and the optical transmittance of 69.1%. Finally, ZAZ/PET multilayer thin film electrode was found to be the lowest sheet resistance of 20.8 Ω/□ and the optical transmittance of 62.0%. The obtained results for the sheet resistance, the surface morphology, the Optical transmittance and the transmittance ratio of the ITO films deposed on PET substrate are reported. Details on the sample preparations and experimental details have been presented.

SEM images and XRD patterns have shown that the surface of the ZTO thin film was smooth and that thin film had an amorphous structure both on SLG and polymer substrates. As results are that the deposition of method DC magnetron sputtering with the coated flexible ZAZ multilayer thin film electrodes will be promising indium-free that it is important to can replace conventional amorphous ITO electrodes. These results indicate that the ZAZ multilayer thin film electrodes with approximately 12.4 nm thick Ag interlayer represents an alternative TCO film that can be utilized in a variety of optoelectronic devices and large flat panel displays. The $ZnSnO_3$/Ag/$ZnSnO_3$ multilayer thin film electrodes were produced by magnetron sputtering. The scanning electron microscopy imageries exposed that ZTO and ZAZ multilayer thin film electrodes were homogeneously on the surfaces of $ZnSnO_3$ thin films. The better sensitivity performance of composites was based on $ZnSnO_3$ thin films with an enormous quantity of oxygen components. As a consequence, we can be used these samples due to understanding the eligibility of ZTO as an anode in OLED production. Thus, these films are promising for flexible OLED applications. We believe that these experimental results will help in the development of transparent conductive oxides with good flexibility, high efficiency, reliability and high-quality levels for optoelectronic devices.

# REFERENCES


Anisotropy, Axial, S Sugano, Y Tanabe, H Kamimura, W H Bauer, Acta Crystallogr, J W Stout, et al. 1970. "OVERLAP CONTRIBUTIONS TO THE Pressure and Temperature Dependences of the Raman-Active Phonons in SnO, ~." *J. Kondo, Prog. Theor. Phys*.

Bädeker, K. 1907. "Über Die Elektrische Leitfähigkeit Und Die Thermoelektrische Kraft Einiger Schwermetallverbindungen." *Annalen Der Physik* 327 (4): 749–66. https://doi.org/10.1002/andp.19073270409.

Bora, Tanujjal, Muna H. Al-Hinai, Ashraf T. Al-Hinai, and Joydeep Dutta. 2015. "Phase Transformation of Metastable ZnSnO3Upon Thermal Decomposition by In-Situ Temperature-Dependent Raman Spectroscopy." *Journal of the American Ceramic Society*. https://doi.org/10.1111/jace.13791.

Bragg, W. H. 1913. "The Reflection of X-Rays by Crystals [3]." *Nature*. https://doi.org/10.1038/091477b0.

Burroughes, J. H., D. D. C. Bradley, A. R. Brown, R. N. Marks, K. Mackay, R. H. Friend, P. L. Burns, and A. B. Holmes. 1990. "Light-Emitting Diodes Based on Conjugated Polymers." *Nature* 347 (6293): 539–41. https://doi.org/10.1038/347539a0.

Castañeda, Luis. 2011. "Present Status of the Development and Application of Transparent Conductors Oxide Thin Solid Films." *Materials Sciences and Applications*. https://doi.org/10.4236/msa.2011.29167.

Chiang, H. Q., J. F. Wager, R. L. Hoffman, J. Jeong, and D. A. Keszler. 2005. "High Mobility Transparent Thin-Film Transistors with Amorphous Zinc Tin Oxide Channel Layer." *Applied Physics Letters*. https://doi.org/10.1063/1.1843286.

Chiang, I. W., B. E. Brinson, R. E. Smalley, J. L. Margrave, and R. H. Hauge. 2001. "Purification and Characterization of Single-Wall Carbon Nanotubes." *The Journal of Physical Chemistry B*. https://doi.org/10.1021/jp003453z.

Choi, Kwang Hyuk, Ho Jun Nam, Jin A. Jeong, Sung Woo Cho, Han Ki Kim, Jae Wook Kang, Do Geun Kim, and Woon Jo Cho. 2008. "Highly Flexible and Transparent InZnSn Ox AgInZnSn Ox Multilayer Electrode for Flexible Organic Light Emitting Diodes." *Applied Physics Letters*. https://doi.org/10.1063/1.2937845.

Choi, Yoon Young, Kwang Hyuk Choi, Hosun Lee, Hosuk Lee, Jae Wook Kang, and Han Ki Kim. 2011. "Nano-Sized Ag-Inserted Amorphous ZnSnO3 Multilayer Electrodes for Cost-Efficient Inverted Organic Solar Cells." *Solar Energy Materials and Solar Cells*. https://doi.org/10.1016/j.solmat.2011.01.013.

Demirhan, Yasemin, Hasan Koseoglu, Fulya Turkoglu, Zemzem Uyanik, Mehtap Ozdemir, Gulnur Aygun, and Lutfi Ozyuzer. 2020."The Controllable Deposition of Large Area Roll-to-Roll Sputtered ITO Thin Films for Photovoltaic Applications."RenewableEnergy146(February):1549–59. https://doi.org/10.1016/j.renene.2019.07.038.

Dixon, Sebastian C., David O. Scanlon, Claire J. Carmalt, and Ivan P. Parkin. 2016. "N-Type Doped Transparent Conducting Binary Oxides: An Overview." *Journal of Materials Chemistry C*. https://doi.org/10.1039/c6tc01881e.

Dsy, Jayathilake, and Nirmal Peiris. 2018. "Overview on Transparent Conducting Oxides and State of the Art of Low-Cost Doped ZnO Systems." *SF Journal of Material and Chemical Engineering*.

Egerton, R. F. 2016. *Physical Principles of Electron Microscopy: An Introduction to TEM, SEM, and AEM, Second Edition*. *Physical Principles of Electron Microscopy: An Introduction to TEM, SEM, and AEM, Second Edition*. https://doi.org/10.1007/978-3-319-39877-8.

Ellmer, Klaus, and Rainald Mientus. 2008. "Carrier Transport in Polycrystalline ITO and ZnO:Al II: The Influence of Grain Barriers and Boundaries." *Thin Solid Films*. https://doi.org/10.1016/j.tsf.2007.10.082.

Exarhos, Gregory J., and Xiao-Dong Zhou. 2007. "Discovery-Based Design of Transparent Conducting Oxide Films." *Thin Solid Films* 515 (18): 7025–52. https://doi.org/10.1016/j.tsf.2007.03.014.

Ghorbani, Mohammad Matboo, and Reza Taherian. 2019. "Methods of Measuring Electrical Properties of Material." In *Electrical Conductivity in Polymer-Based Composites: Experiments, Modelling and Applications*, 365–94. Elsevier. https://doi.org/10.1016/B978-0-12-812541-0.00012-4.

Ginley, David S., ed. 2011. *Handbook of Transparent Conductors*. *Handbook of Transparent Conductors*. Boston, MA: Springer US. https://doi.org/10.1007/978-1-4419-1638-9.

Granqvist, C. G., and A. Hultåker. 2002. "Transparent and Conducting ITO Films: New DevelopmentsandApplications."In*ThinSolidFilms*.https://doi.org/10.1016/S0040-6090(02)00163-3.

Helfrich, W., and W. G. Schneider. 1965. "Recombination Radiation in Anthracene Crystals." *Physical Review Letters*. https://doi.org/10.1103/PhysRevLett.14.229.

Hung, L. S., and C. H. Chen. 2002. "Recent Progress of Molecular Organic Electroluminescent Materials and Devices." *Materials Science and Engineering*

*R: Reports*. https://doi.org/10.1016/S0927-796X(02)00093-1.

Kim, Sung Il, Kyo Woong Lee, Bibhuti Bhusan Sahu, and Jeon Geon Han. 2015. "Flexible OLED Fabrication with ITO Thin Film on Polymer Substrate." *Japanese Journal of Applied Physics*. https://doi.org/10.7567/JJAP.54.090301.

Klaassen, F. M., and W. Hes. 1986. "On the Temperature Coefficient of the MOSFET Threshold Voltage." *Solid State Electronics*. https://doi.org/10.1016/0038-1101(86)90180-2.

Koseoglu, Hasan, Fulya Turkoglu, Metin Kurt, Mutlu D. Yaman, Fatime G. Akca, Gulnur Aygun, and Lutfi Ozyuzer. 2015. "Improvement of Optical and Electrical Properties of ITO Thin Films by Electro-Annealing." *Vacuum* 120: 8–13. https://doi.org/10.1016/j.vacuum.2015.06.027.

Lewis, Brian G., and David C. Paine. 2000. "Applications and Processing of Transparent Conducting Oxides." *MRS Bulletin*. https://doi.org/10.1557/mrs2000.147.

Major, S., and K. L. Chopra. 1988. "Indium-Doped Zinc Oxide Films as Transparent Electrodes for Solar Cells." *Solar Energy Materials*. https://doi.org/10.1016/0165-1633(88)90014-7.

Mereu, R. A., A. Le Donne, S. Trabattoni, M. Acciarri, and S. Binetti. 2015. "Comparative Study on Structural, Morphological and Optical Properties of Zn2SnO4 Thin Films Prepared by r.f. Sputtering Using Zn and Sn Metal Targets and ZnO-SnO2 Ceramic Target." *Journal of Alloys and Compounds*. https://doi.org/10.1016/j.jallcom.2014.11.150.

Minami, Tadatsugu. 2005. "Transparent Conducting Oxide Semiconductors for Transparent Electrodes." *Semiconductor Science and Technology*. https://doi.org/10.1088/0268-1242/20/4/004.

Parthasarathy, G, J Liu, and A R Duggal. 2003. "Organic Light Emitting Devices from Displays to Lighting." *Electrochemical Society Interface* 12 (2): 42–47. https://www.scopus.com/inward/record.url?eid=2-s2.0-0037828609&partnerID=40&md5=115dbca42f2eeb83ab0bca189f020de8.

Pasquarelli, Robert M., David S. Ginley, and Ryan O'Hayre. 2011. "Solution Processing of Transparent Conductors: From Flask to Film." *Chemical Society Reviews*. https://doi.org/10.1039/c1cs15065k.

Saafi, I., R. Dridi, R. Mimouni, A. Amlouk, A. Yumak, K. Boubaker, P. Petkova, and M. Amlouk. 2016. "Microstructural and Optical Properties of SnO2-ZnSnO3 Ceramics."*CeramicsInternational*.https://doi.org/10.1016/j.ceramint.2016.01.010

Schmidt, H., T. Winkler, I. Baumann, S. Schmale, H. Flügge, H. H. Johannes, S. Hamwi, T. Rabe, T. Riedl, and W. Kowalsky. 2011. "Indium-Free Bottom Electrodes for Inverted Organic Solar Cells with Simplified Cell Architectures." *Applied Physics Letters*. https://doi.org/10.1063/1.3610997.

Schroder, Dieter K. 2005. *Semiconductor Material and Device Characterization: Third Edition*. *Semiconductor Material and Device Characterization: Third Edition*. https://doi.org/10.1002/0471749095.

Scott, J. F. 1970. "Raman Spectrum of SnO2." *The Journal of Chemical Physics*. https://doi.org/10.1063/1.1674079.

Seok, Hae-Jun, Hyeon-Woo Jang, Dong-Yeop Lee, Beom-Gwon Son, and Han-Ki Kim. 2019. "Roll-to-Roll Sputtered, Indium-Free ZnSnO/AgPdCu/ZnSnO Multi-Stacked Electrodes for High Performance Flexible Thin-Film Heaters and Heat-Shielding Films." *Journal of Alloys and Compounds* 775 (February): 853–64. https://doi.org/10.1016/j.jallcom.2018.10.194.

Shirota, Yasuhiko, and Hiroshi Kageyama. 2007. "Charge Carrier Transporting Molecular Materials and Their Applications in Devices." *Chemical Reviews* 107 (4): 953–1010. https://doi.org/10.1021/cr050143+.

Stambolova, I., K. Konstantinov, D. Kovacheva, P. Peshev, and T. Donchev. 1997. "Spray Pyrolysis Preparation and Humidity Sensing Characteristics of Spinel Zinc Stannate Thin Films." *Journal of Solid State Chemistry*. https://doi.org/10.1006/jssc.1996.7174.

Tang, C. W., and S. A. VanSlyke. 1987. "Organic Electroluminescent Diodes." *Applied Physics Letters* 51 (12): 913–15. https://doi.org/10.1063/1.98799.

Thejo Kalyani, N., and S. J. Dhoble. 2015. "Novel Materials for Fabrication and Encapsulation of OLEDs." *Renewable and Sustainable Energy Reviews*. https://doi.org/10.1016/j.rser.2014.11.070.

Tuna, Ocal, Yusuf Selamet, Gulnur Aygun, and Lutfi Ozyuzer. 2010. "High Quality ITO Thin Films Grown by Dc and RF Sputtering without Oxygen." *Journal of Physics D: Applied Physics* 43 (5). https://doi.org/10.1088/0022-3727/43/5/055402.

Turkoglu, F., H. Koseoglu, S. Zeybek, M. Ozdemir, G. Aygun, and L. Ozyuzer. 2018. "Effect of Substrate Rotation Speed and Off-Center Deposition on the Structural, Optical, and Electrical Properties of AZO Thin Films Fabricated by DC Magnetron Sputtering." *Journal of Applied Physics*. https://doi.org/10.1063/1.5012883.

Wei, S, and D Segev. 2005. "Electronic and Optical Properties of Spinel TCOs :

SnZn2O4, SnCd2O4, and CdIn2O4." In *DOE Solar Energy Technologies*.

Welzel, Thomas, and Klaus Ellmer. 2012. "Negative Oxygen Ion Formation in Reactive Magnetron Sputtering Processes for Transparent Conductive Oxides." *Journal of Vacuum Science & Technology A: Vacuum, Surfaces, and Films*. https://doi.org/10.1116/1.4762815.

Yahia, S. Ben, L. Znaidi, A. Kanaev, and J. P. Petitet. 2008. "Raman Study of Oriented ZnO Thin Films Deposited by Sol-Gel Method." *Spectrochimica Acta - Part A: Molecular and Biomolecular Spectroscopy*. https://doi.org/10.1016/j.saa.2008.03.032.

Zeng, Kaiyang, Furong Zhu, Jianqiao Hu, Lu Shen, Keran Zhang, and Hao Gong. 2003. "Investigation of Mechanical Properties of Transparent Conducting Oxide Thin Films." *Thin Solid Films*. https://doi.org/10.1016/S0040-6090(03)00915-5.